

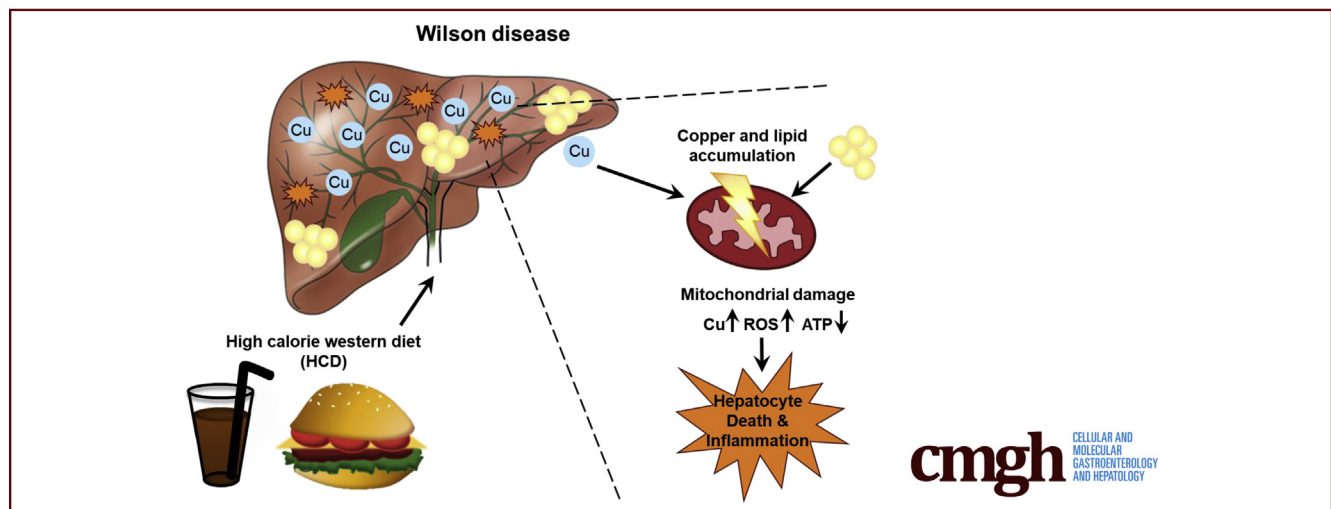
## ORIGINAL RESEARCH

## A High-Calorie Diet Aggravates Mitochondrial Dysfunction and Triggers Severe Liver Damage in Wilson Disease Rats



Claudia Einer,<sup>1,2,\*</sup> Christin Leitzinger,<sup>1,\*</sup> Josef Lichtmanegger,<sup>1</sup> Carola Eberhagen,<sup>1</sup> Tamara Rieder,<sup>3</sup> Sabine Borchard,<sup>1</sup> Ralf Wimmer,<sup>2</sup> Gerald Denk,<sup>2</sup> Bastian Popper,<sup>4,5</sup> Frauke Neff,<sup>6</sup> Elena V. Polishchuk,<sup>7</sup> Roman S. Polishchuk,<sup>7</sup> Stefanie M. Hauck,<sup>8</sup> Christine von Toerne,<sup>8</sup> Jennifer-Christin Müller,<sup>9</sup> Uwe Karst,<sup>9</sup> Bipin S. Baral,<sup>10</sup> Alan A. DiSpirito,<sup>10</sup> Andreas E. Kremer,<sup>11</sup> Jeremy Semrau,<sup>12</sup> Karl Heinz Weiss,<sup>13</sup> Simon Hohenester,<sup>2,§</sup> and Hans Zischka<sup>1,3,§</sup>

<sup>1</sup>Institute of Molecular Toxicology and Pharmacology, <sup>6</sup>Institute of Pathology, <sup>8</sup>Research Unit Protein Science, Helmholtz Center Munich, German Research Center for Environmental Health, Neuherberg, Germany; <sup>2</sup>Department of Medicine II, University Hospital, Ludwig-Maximilians-University Munich, Munich, Germany; <sup>3</sup>Institute of Toxicology and Environmental Hygiene, Technical University Munich, Munich, Germany; <sup>4</sup>Department of Anatomy and Cell Biology, <sup>5</sup>Core Facility Animal Models, Biomedical Center, Ludwig-Maximilians-University, Planegg-Martinsried, Germany; <sup>7</sup>Telethon Institute of Genetics and Medicine, Pozzuoli (Naples), Italy; <sup>9</sup>Institute of Inorganic and Analytical Chemistry, University of Münster, Münster, Germany; <sup>10</sup>Roy J. Carver Department of Biochemistry, Biophysics and Molecular Biology, Iowa State University, Ames, Iowa; <sup>11</sup>Department of Medicine I, Friedrich-Alexander-University Erlangen-Nürnberg, Erlangen, Germany; <sup>12</sup>Department of Civil and Environmental Engineering, University of Michigan, Ann Arbor, Michigan; <sup>13</sup>Department of Gastroenterology, Internal Medicine IV, University Hospital Heidelberg, Heidelberg, Germany



## SUMMARY

A high-calorie diet severely aggravates hepatic mitochondrial and hepatocellular damage in Wilson disease rats. A toxic triad of adenosine triphosphate depletion, increased reactive oxygen species, and increased bile salts lead to an earlier onset of the disease and to enhanced disease progression.

**BACKGROUND & AIMS:** In Wilson disease, *ATP7B* mutations impair copper excretion into bile. Hepatic copper accumulation may induce mild to moderate chronic liver damage or even acute liver failure. Etiologic factors for this heterogeneous phenotype remain enigmatic. Liver steatosis is a frequent finding in Wilson disease patients, suggesting that impaired

copper homeostasis is linked with liver steatosis. Hepatic mitochondrial function is affected negatively both by copper overload and steatosis. Therefore, we addressed the question of whether a steatosis-promoting high-calorie diet aggravates liver damage in Wilson disease via amplified mitochondrial damage.

**METHODS:** Control *Atp7b*<sup>+/+</sup> and Wilson disease *Atp7b*<sup>-/-</sup> rats were fed either a high-calorie diet (HCD) or a normal diet. Copper chelation using the high-affinity peptide methanobactin was used in HCD-fed *Atp7b*<sup>-/-</sup> rats to test for therapeutic reversal of mitochondrial copper damage.

**RESULTS:** In comparison with a normal diet, HCD feeding of *Atp7b*<sup>-/-</sup> rats resulted in a markedly earlier onset of clinically apparent hepatic injury. Strongly increased mitochondrial copper accumulation was observed in HCD-fed *Atp7b*<sup>-/-</sup> rats, correlating with severe liver injury. Mitochondria presented

with massive structural damage, increased H<sub>2</sub>O<sub>2</sub> emergence, and dysfunctional adenosine triphosphate production. Hepatocellular injury presumably was augmented as a result of oxidative stress. Reduction of mitochondrial copper by methanobactin significantly reduced mitochondrial impairment and ameliorated liver damage.

**CONCLUSIONS:** A high-calorie diet severely aggravates hepatic mitochondrial and hepatocellular damage in Wilson disease rats, causing an earlier onset of the disease and enhanced disease progression. (*Cell Mol Gastroenterol Hepatol* 2019;7:571–596; <https://doi.org/10.1016/j.jcmgh.2018.12.005>)

**Keywords:** Copper-Storage Disease; Steatosis; Steatohepatitis; Mitochondria; Methanobactin.

See editorial on page 684.

**W**ilson disease (WD) is an autosomal-recessively inherited disorder of copper metabolism caused by *ATP7B* gene mutations, resulting in impaired biliary copper excretion. Subsequent hepatic copper accumulation induces a heterogeneous phenotype that lacks a clear genotype correlation.<sup>1</sup> Although some individuals remain rather unaffected, others develop mild to moderate chronic liver disease or even acute liver failure.<sup>2</sup> The mechanisms underlying this heterogeneity are currently unknown. Pharmacologic therapies in WD aim to restore copper homeostasis.<sup>2</sup> In *Atp7b*<sup>-/-</sup> rats, an animal model mirroring the WD liver phenotype,<sup>3</sup> hepatic copper accumulation causes a reduced mitochondrial adenosine triphosphate (ATP) production capacity, mitochondrial destruction, liver failure, and animal death.<sup>4,5</sup> Heterozygous *Atp7b*<sup>+/-</sup> rats do not accumulate copper and thus are highly stringent, nonaffected control animals.<sup>3,4</sup> Copper-induced mitochondrial damage in *Atp7b*<sup>-/-</sup> rats can be resolved efficiently by innovative treatments using the potent copper chelating agent methanobactin (MB),<sup>5</sup> which has an extraordinarily high copper affinity.<sup>6,7</sup> MB decreases mitochondrial copper within days, coinciding with liver tissue restoration and avoidance of liver failure and animal death.<sup>5</sup>

Besides mitochondrial impairments, fat accumulation (steatosis) is a frequently observed early characteristic in livers of WD patients.<sup>8,9</sup> Indeed, WD often may be misdiagnosed as nonalcoholic fatty liver disease (NAFLD).<sup>9</sup> The prevalence of NAFLD is increasing in Western societies, in many cases owing to high-calorie malnutrition (ie, excessive intake of fat and sugar), and the associated metabolic syndrome.<sup>10</sup> Interestingly, in NAFLD patients, mitochondrial alterations similar to those found in WD patients have been reported (eg, altered cristae and reduced ATP production resulting from oxidative phosphorylation defects).<sup>11,12</sup> Wild-type mice subjected to a high-fat, high-fructose-containing diet have functional deficits in their hepatic mitochondria, most prominently a reduced ATP production capacity.<sup>13,14</sup> Thus, mitochondrial structural and functional

impairments are hallmarks in both WD and NAFLD, suggesting a potential link between aberrant hepatic copper and lipid metabolism.


An obvious dietary recommendation for WD patients is to avoid copper-rich foods (eg, shellfish, nuts, or chocolate) to counteract an excessive hepatic copper accumulation.<sup>15</sup> However, much less attention is given to other aspects of WD patient nutrition<sup>16</sup> (eg, fat or sugar content in their diet). The potential influence of such environmental aspects on WD progression and severity came to our attention by a case report on monozygotic WD twins.<sup>17</sup> One of the twins with nutritional disturbance (bulimia nervosa) had clinically apparent signs of liver failure (eg, ongoing hepatocyte necrosis), and had to undergo liver transplantation. Her twin sister, however, underwent a prolonged period of undernourishment, and presented with asymptomatic mild liver disease.<sup>17</sup> This (and further case reports) suggests that lifestyle may impact WD progression, possibly contributing to differing WD phenotypes and to the conundrum of a lacking genotype–phenotype correlation in WD.<sup>18</sup>

Similar to the clinical situation, in WD research, treatments of relevant animal models have plausibly focused on the amelioration of copper-induced liver damage (eg, with the aim to avoid oxidative liver damage).<sup>19,20</sup> The opposite, that is, studies on diets that may aggravate disease progression, are virtually nonexistent. Only recently have reports suggested that misbalanced copper homeostasis participates in liver steatosis and may negatively influence not only lipid and cholesterol metabolism, but also the assembly and secretion of lipoproteins from intestinal enterocytes.<sup>21–23</sup>

Driven by these findings and considerations, we asked whether malnutrition with a high-calorie diet (HCD), enriched in fat and sugar, would influence disease progression in *Atp7b*<sup>-/-</sup> rats. We applied a variant of an HCD that particularly reflects the eating habits in Western society, causing the “American Lifestyle-induced Obesity Syndrome,”<sup>24</sup> and that represents a physiologically relevant, true-to-life-model. The rationale of this study was that both enriched copper and fatty acids cause bioenergetic defects and therefore synergistically and detrimentally may coincide on hepatic mitochondria, which was found to be the case. We thus report here that an HCD accelerated and

\*Authors share co-first authorship; §Authors share co-senior authorship.

**Abbreviations used in this paper:** Acetyl-CoA, acetyl coenzyme A; ADP, adenosine diphosphate; AST, aspartate aminotransferase; ATP, adenosine triphosphate; BSA, bovine serum albumin; Cp, ceruloplasmin; CS, citrate synthase; EGTA, ethylene glycol-bis(β-aminoethyl ether)-N,N,N',N'-tetraacetic acid; F<sub>1</sub>F<sub>0</sub>, adenosine triphosphate synthase; HAI, Histologic Activity Index; HCD, high-calorie diet; ICP, Inductively Coupled Plasma; MB, methanobactin; MS, mass spectrometry; NADH, reduced nicotinamide adenine dinucleotide; NAFLD, nonalcoholic fatty liver disease; NAS, nonalcoholic fatty liver disease activity score; ND, normal diet; ROS, reactive oxygen species; TRIS, tris-(hydroxymethyl)aminomethane; WD, Wilson disease.

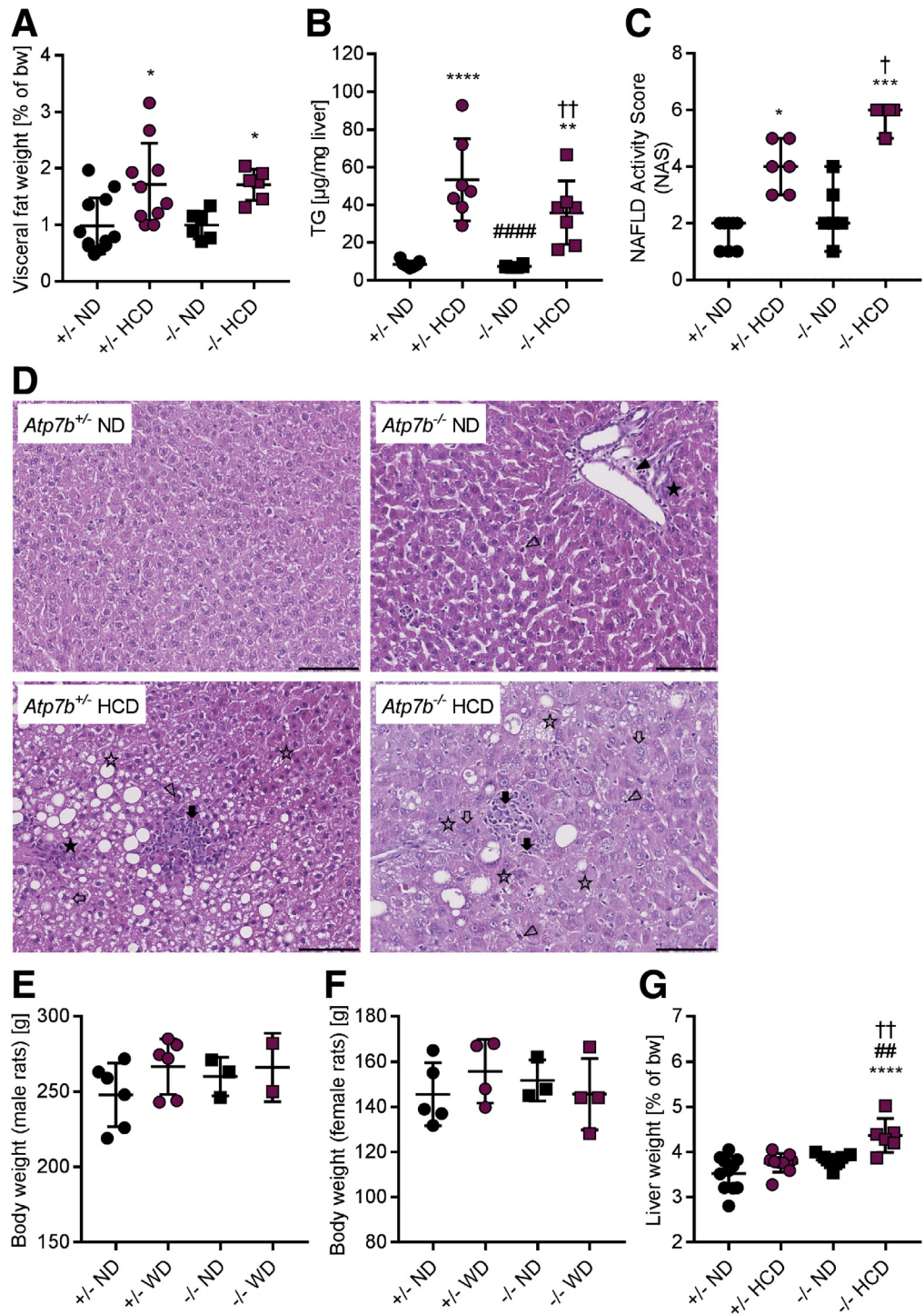
 Most current article

© 2019 The Authors. Published by Elsevier Inc. on behalf of the AGA Institute. This is an open access article under the CC BY-NC-ND license (<http://creativecommons.org/licenses/by-nc-nd/4.0/>).

2352-345X

<https://doi.org/10.1016/j.jcmgh.2018.12.005>

**Figure 1. An HCD induces liver steatosis in *Atp7b*<sup>+/-</sup> and *Atp7b*<sup>-/-</sup> rats.** (A–C) An HCD increases (A) visceral fat mass (N = 6–12), (B) liver triglyceride content (N = 6–7), and (C) NAFLD activity (NAS, N = 6–8) in *Atp7b*<sup>+/-</sup> and *Atp7b*<sup>-/-</sup> rats. (D) Liver histology (H&E stain; scale bar: 100 μm) from ND-fed vs HCD-fed *Atp7b*<sup>+/-</sup> and *Atp7b*<sup>-/-</sup> rats presents macrosteatosis (open asterisk), ballooned hepatocytes (open arrow), inflammatory infiltrations (black arrow), and some signs of fibrosis (black asterisk), apoptosis (open arrowhead), or necrosis (black arrowhead). (E and F) Comparable body weights of either male (E, N = 2–7) or female (F, N = 3–5) ND- or HCD-fed *Atp7b*<sup>+/-</sup> and *Atp7b*<sup>-/-</sup> rats. (G) Relative liver weight (% of body weight [bw]) of HCD-fed *Atp7b*<sup>-/-</sup> rats increased compared with ND-fed *Atp7b*<sup>-/-</sup> and *Atp7b*<sup>+/-</sup> rats (N = 6–11). One-way analysis of variance with (A, B, E–G) the Tukey multiple comparisons test, or (C) the nonparametric Kruskal–Wallis test. N, number of analyzed animals. \*Significant to *Atp7b*<sup>+/-</sup> ND. #Significant to *Atp7b*<sup>+/-</sup> HCD. †Significant to *Atp7b*<sup>-/-</sup> ND. \*,#†P < .05; \*\*,###,††P < .01; \*\*\*,####,†††P < .001; \*\*\*\*,#####,††††P < .0001. TG, triglyceride.



aggravated liver damage in *Atp7b*<sup>-/-</sup> rats. In comparison with *Atp7b*<sup>-/-</sup> rats fed a normal diet (ND), profoundly increased mitochondrial copper accumulation caused severe bioenergetic defects in HCD-fed *Atp7b*<sup>-/-</sup> rats. We conclude that lipid accumulation in copper-burdened hepatocytes may represent a second hit in WD, inducing liver damage, and suggest that further research should establish whether dietary counseling of WD patients may be of therapeutic benefit.

## Results

### An HCD Severely Aggravates and Strongly Accelerates Liver Damage in WD Rats

An HCD significantly increased the visceral fat mass (Figure 1A) and liver triglyceride levels (Figure 1B) within a few weeks of feeding in *Atp7b*<sup>+/-</sup> control rats, compared with their ND-fed counterparts. This coincided with the



**Table 1.** Histologic Assessment of Steatosis, Lobular Inflammation, and Hepatocyte Ballooning (NAS) in Livers of ND- and HCD-Fed *Atp7b*<sup>+/-</sup> and *Atp7b*<sup>-/-</sup> Rats

NAS		Genotype									
		+/-	+/-	+/-	+/-	+/-	+/-	+/-	+/-	+/-	+/-
		Chow		ND		ND		ND		HCD	
		Animal ID	Rat 3	Rat 15	Rat 1	Rat 2	Rat 14	Rat 16	Rat 17	Rat 20	Rat 5
Steatosis grade	<5%	0	0	0	0	0	0	0	0	0	0
	5%–33%	1									1
	>33% to 66%	2									
	>66%	3									
Lobular inflammation	No foci	0			0						
	<2 foci per 200× field	1	1	1		1	1	1	1	1	1
	2–4 foci per 200× field	2									
	>4 foci per 200× field	3									
Ballooning	None	0				0		0			
	Few balloon cells	1	1	1	1		1		1	1	1
	Many cells/ prominent ballooning	2									
Diagnostic classification (NAS)											
	Not steatohepatitis	<3	2	2	1	1	2	1	2	2	
	Possible/ borderline	3–4									3
	Definite steatohepatitis	≥5									

presence of abundant macrosteatosis in liver histology (Figure 1D) and an increased NAFLD Activity Score (NAS) of 3–5 (Figure 1C, Table 1). Despite steatosis, however, constant body and liver weights were encountered in the HCD-fed control *Atp7b*<sup>+/-</sup> rats (Figure 1E–G, Table 2). HCD- vs ND-fed *Atp7b*<sup>-/-</sup> rats (ie, WD rats) also had tendentially increased visceral fat mass, significantly increased liver triglyceride levels, liver steatosis, and equal body but increased liver weight (Figures 1A–G, Table 2).

Importantly, clinically apparent liver injury (ie, serum aspartate aminotransferase [AST] level, >200 U/L) was present only in age-matched HCD-fed *Atp7b*<sup>-/-</sup> rats, but not in ND-fed *Atp7b*<sup>-/-</sup> or in HCD-fed *Atp7b*<sup>+/-</sup> rats (Figure 2A, Table 2). Gross liver damage was further detectable by histologic analyses only in HCD-fed *Atp7b*<sup>-/-</sup>, but not in the other groups (Figures 1D, 2C and D, Table 3). Although in the other groups, single necrosis and apoptosis, low signs of inflammation or fibrosis, occasionally were observed, these features became severely apparent and increased significantly (vs ND-fed controls) only in HCD-fed *Atp7b*<sup>-/-</sup> rats (Figure 2C and D, Tables 1 and 3). Summation of these parameters resulted in low NAS and Histologic Activity Index (HAI) scores for the other rats, but showed strongly and significantly (vs both ND-fed controls and ND-fed *Atp7b*<sup>-/-</sup> rats) increased NAS and HAI scores for HCD-fed *Atp7b*<sup>-/-</sup> rats (Figures 1C and 2C). Because steatosis, hepatocyte ballooning, and inflammation are the hallmarks of nonalcoholic steatohepatitis,<sup>25</sup> such nonalcoholic steatohepatitis was present in all 6 HCD-fed *Atp7b*<sup>-/-</sup> rats, but in only 2 of 6 HCD-fed *Atp7b*<sup>+/-</sup> rats (Table 1).

With respect to WD, we further tested for a difference in disease progression in HCD- vs ND-fed *Atp7b*<sup>-/-</sup> rats. As can be seen in Figure 2B, HCD feeding led to a earlier disease

onset by approximately 20 days in HCD- vs ND-fed *Atp7b*<sup>-/-</sup> rats. This is a remarkable disease acceleration, because earlier we had determined a median survival of 106 days in ND-fed *Atp7b*<sup>-/-</sup> rats.<sup>4</sup> In addition, a noticeable steeper slope of the trend curve for liver damage was observed in HCD- vs ND-fed *Atp7b*<sup>-/-</sup> rats (Figure 2B). Thus, HCD feeding causes severely aggravated liver damage that appears much earlier and progresses faster in HCD- vs ND-fed *Atp7b*<sup>-/-</sup> rats.

### An HCD Increases Serum and Mitochondrial Copper Load in *Atp7b*<sup>-/-</sup> Rats

In WD livers, copper-loading of ceruloplasmin (Cp) is impaired because of *ATP7B* mutations.<sup>2</sup> Consequently, Cp oxidase activity and copper concentrations in peripheral blood typically are reduced.<sup>26</sup> Accordingly, ND-fed *Atp7b*<sup>-/-</sup> rats presented almost no Cp oxidase activity and significantly decreased plasma copper levels compared with *Atp7b*<sup>+/-</sup> controls (Figure 3A and B). Of note, HCD feeding of *Atp7b*<sup>+/-</sup> rats resulted in significantly lower serum copper and Cp oxidase activity compared with ND-fed controls (Figure 3A and B). This is in line with observations in NAFLD patients, in whom reduced Cp oxidase activity was found to be associated strongly with hepatocyte ballooning or liver steatosis and therefore was suggested as a potential marker of liver dysfunction in fatty liver injury.<sup>27,28</sup> In contrast to *Atp7b*<sup>+/-</sup> control rats, HCD feeding of *Atp7b*<sup>-/-</sup> rats still resulted in low Cp oxidase activity (Figure 3A), but in a significant increase of serum copper if compared with ND-fed *Atp7b*<sup>-/-</sup> rats (Figure 3B). Such increased non-Cp bound serum copper is a hallmark of overt liver damage in WD<sup>2</sup> that may arise from disintegrated hepatocytes, because

**Table 1.** Continued

+/-	+/-	+/-	+/-	+/-	-/-	-/-	-/-	-/-	-/-	-/-	-/-	-/-	-/-	-/-	-/-	-/-
HCD	HCD	HCD	HCD	HCD	ND	ND	ND	ND	ND	ND	HCD	HCD	HCD	HCD	HCD	HCD
Rat 4	Rat 6	Rat 24	Rat 23	Rat 27	Rat 31	Rat 8	Rat 7	Rat 9	Rat 29	Rat 30	Rat 11	Rat 10	Rat 12	Rat 35	Rat 36	Rat 37
					0	0	0	0	0	0						
	1	1		1									1	1	1	1
2			2								2	2				
1		1			1			1		1						
	2		2	2			2		2		2	2	2			
						3								3	3	3
							0			0						
1		1	1	1	1	1		1	1							
	2										2	2	2	2	2	2
						2	2	2		1						
4		3		4		4			3							
	5		5								6	6	5	6	6	6

necrosis was largely present in the HCD-fed *Atp7b*<sup>-/-</sup> rats (Figure 2D).

WD *Atp7b*<sup>-/-</sup> rats, either ND- or HCD-fed, accumulated comparable copper amounts in whole liver homogenates and liver cytosol (Figure 3C and D). This finding shows a comparable copper intake via the ND/tap water diet vs the HCD/sugar water diet, respectively. In contrast, however, an excessive increase in copper was found in mitochondria isolated from HCD- vs ND-fed *Atp7b*<sup>-/-</sup> rats (Figure 3E). Of note, a significant increase in mitochondrial copper also was determined in HCD- vs ND-fed control *Atp7b*<sup>+/-</sup> rats. Importantly, such increased mitochondrial copper significantly correlated with a higher NAS and a progressive HAI score (Figure 3F).

**An HCD Strongly Amplifies Hepatic Mitochondrial Damage in *Atp7b*<sup>-/-</sup> Rats**

Structural and functional alterations in liver mitochondria are early key features in WD patients<sup>5,8,29</sup> and related animal models.<sup>5,30</sup> Mitochondrial alterations also are prominent features in NAFLD patients<sup>11,12</sup> and related animal models.<sup>13,31</sup> We therefore hypothesized that the combined effect of genetically driven copper accumulation owing to the *Atp7b* knockout and metabolic disturbance induced by the high-calorie nutrition may accelerate the deterioration of hepatic mitochondria.

In full agreement with this supposition, feeding *Atp7b*<sup>-/-</sup> rats with an HCD severely affected their hepatic mitochondria (Figure 4). Compared with mitochondria from ND-fed *Atp7b*<sup>-/-</sup> rats and from control (*Atp7b*<sup>+/-</sup>) rats, mitochondria from HCD-fed *Atp7b*<sup>-/-</sup> rats appeared with detached inner and outer membranes, prominent matrix

condensations, and ballooned cristae (Figure 4A and B, arrows). Such typical WD features were partly observed in mitochondria from age-matched ND-fed *Atp7b*<sup>-/-</sup> rats, albeit to a significantly lower extent (Figure 4B, and quantification in 4C). In contrast to mitochondria from ND-fed *Atp7b*<sup>+/-</sup> rats, HCD-fed *Atp7b*<sup>+/-</sup> mitochondria had partly rounded vesicular cristae that also were abundantly present in HCD-fed *Atp7b*<sup>-/-</sup> mitochondria (Figure 4A and B, asterisks). Thus, hepatic mitochondria are affected in structure by both copper deposition and HCD, and their combination resulted in a most severe mitochondrial phenotype.

These structural impairments were paralleled by remarkable mitochondrial functional deficits. The capacity to produce ATP was significantly lower in mitochondria from either HCD-fed *Atp7b*<sup>+/-</sup> or ND-fed *Atp7b*<sup>-/-</sup> rats in comparison with those from ND-fed *Atp7b*<sup>+/-</sup> controls (Figure 5A). However, the strongest decrease in ATP production capacity was determined in mitochondria from HCD-fed *Atp7b*<sup>-/-</sup> rats, in which ATP production capacity was significantly lower than in all other tested mitochondrial populations (Figure 5A). In addition, the lowest, albeit not significantly decreased, mean ATP synthase (F<sub>1</sub>F<sub>0</sub>) activity was found in mitochondria from HCD-fed *Atp7b*<sup>-/-</sup> rats (Figure 5B). In contrast, HCD feeding hardly affected mitochondrial oxygen consumption (Figure 5C) and did not change respiratory control ratios (Figure 5D) because only nonsignificant tendencies for increased succinate-linked, leak, and maximum oxygen consumption rates were observed in the restricted number of investigated HCD- vs ND-fed animals. It thus remains for future studies to evaluate whether these alterations do or do not contribute to mitochondrial dysfunction in HCD-fed *Atp7b*<sup>-/-</sup> rats.

**Table 2.** An HCD Accelerates Disease Progression in *Atp7b*<sup>-/-</sup> Rats

Animal ID	Genotype	Chow	Age, days	Sex	Body weight, g	AST, U/L	Bilirubin, mg/dL
Rat 1	+/-	ND	67	M	206	181	<0.5
Rat 2	+/-	ND	73	F	132	146	<0.5
Rat 3	+/-	ND	75	F	155	137	<0.5
Rat 4	+/-	HCD	67	F	148	108	<0.5
Rat 5	+/-	HCD	73	F	140	125	<0.5
Rat 6	+/-	HCD	75	F	167	127	<0.5
Rat 7	-/-	ND	67	M	214	152	<0.5
Rat 8	-/-	ND	73	F	148	181	<0.5
Rat 9	-/-	ND	75	F	145	130	<0.5
Rat 10	-/-	HCD	67	F	144	122	<0.5
Rat 11	-/-	HCD	73	F	128	318 <sup>a</sup>	<0.5
Rat 12	-/-	HCD	75	F	144	298 <sup>a</sup>	<0.5
Rat 13	+/-	ND	79	M	259	93.5	<0.5
Rat 14	+/-	ND	79	F	137	93.1	<0.5
Rat 15	+/-	ND	80	F	139	95.8	<0.5
Rat 16	+/-	ND	80	F	165	73.6	<0.5
Rat 17	+/-	ND	81	M	272	78.5	<0.5
Rat 18	+/-	ND	81	M	219	96.5	<0.5
Rat 19	+/-	ND	81	M	248	222	<0.5
Rat 20	+/-	ND	82	M	263	156	<0.5
Rat 21	+/-	ND	82	M	226	123	<0.5
Rat 22	+/-	HCD	79	M	285	90.4	<0.5
Rat 23	+/-	HCD	80	F	168	65.2	<0.5
Rat 24	+/-	HCD	81	M	281	69.9	<0.5
Rat 25	+/-	HCD	81	M	272	77.6	<0.5
Rat 26	+/-	HCD	81	M	244	123	<0.5
Rat 27	+/-	HCD	82	M	275	139	<0.5
Rat 28	+/-	HCD	82	M	243	125	<0.5
Rat 29	-/-	ND	80	F	162	82.2	<0.5
Rat 30	-/-	ND	81	M	271	80.5	<0.5
Rat 31	-/-	ND	82	M	263	115	<0.5
Rat 32	-/-	ND	82	M	246	141	<0.5
Rat 33	-/-	ND	82	M	264	90.2	<0.5
Rat 34	-/-	ND	82	M	262	117	<0.5
Rat 35	-/-	HCD	80	F	167	460 <sup>a</sup>	4.4 <sup>a</sup>
Rat 36	-/-	HCD	81	M	250	486 <sup>a</sup>	<0.5
Rat 37	-/-	HCD	82	M	282	610 <sup>a</sup>	1.8 <sup>a</sup>

F, female; M, male.

<sup>a</sup>Animals are considered as having clinically apparent WD if AST level is greater than 200 U/L and/or bilirubin level is greater than 0.5 mg/dL.

Importantly, mitochondria from HCD-fed *Atp7b*<sup>-/-</sup> rats appeared with 2 highly cell-toxic features that were changed significantly in comparison with the mitochondrial populations from all other rats. The first was a significantly lower ATP production (Figure 5A), and the second was that only mitochondria from HCD-fed *Atp7b*<sup>-/-</sup> rats showed significantly enhanced mitochondrial H<sub>2</sub>O<sub>2</sub> emergence, whether tested with either respiratory complex II-linked succinate (Figure 5E) or with respiratory complex I-linked glutamate/malate (Figure 5F) as substrates. Appreciable mitochondrial

reactive oxygen species (ROS) were neither emerging from mitochondria from (still) healthy ND-fed WD rats nor from HCD-fed control rats, but were exclusive features of severely damaged mitochondria in HCD-fed *Atp7b*<sup>-/-</sup> rats.

#### *An HCD Increases Enzyme Abundancies of Hepatic Lipid and Bile Salt Synthesis in *Atp7b*<sup>-/-</sup> Rats*

How does the combined challenge of decreased copper excretion (owing to *Atp7b* deletion) and increased fatty acid

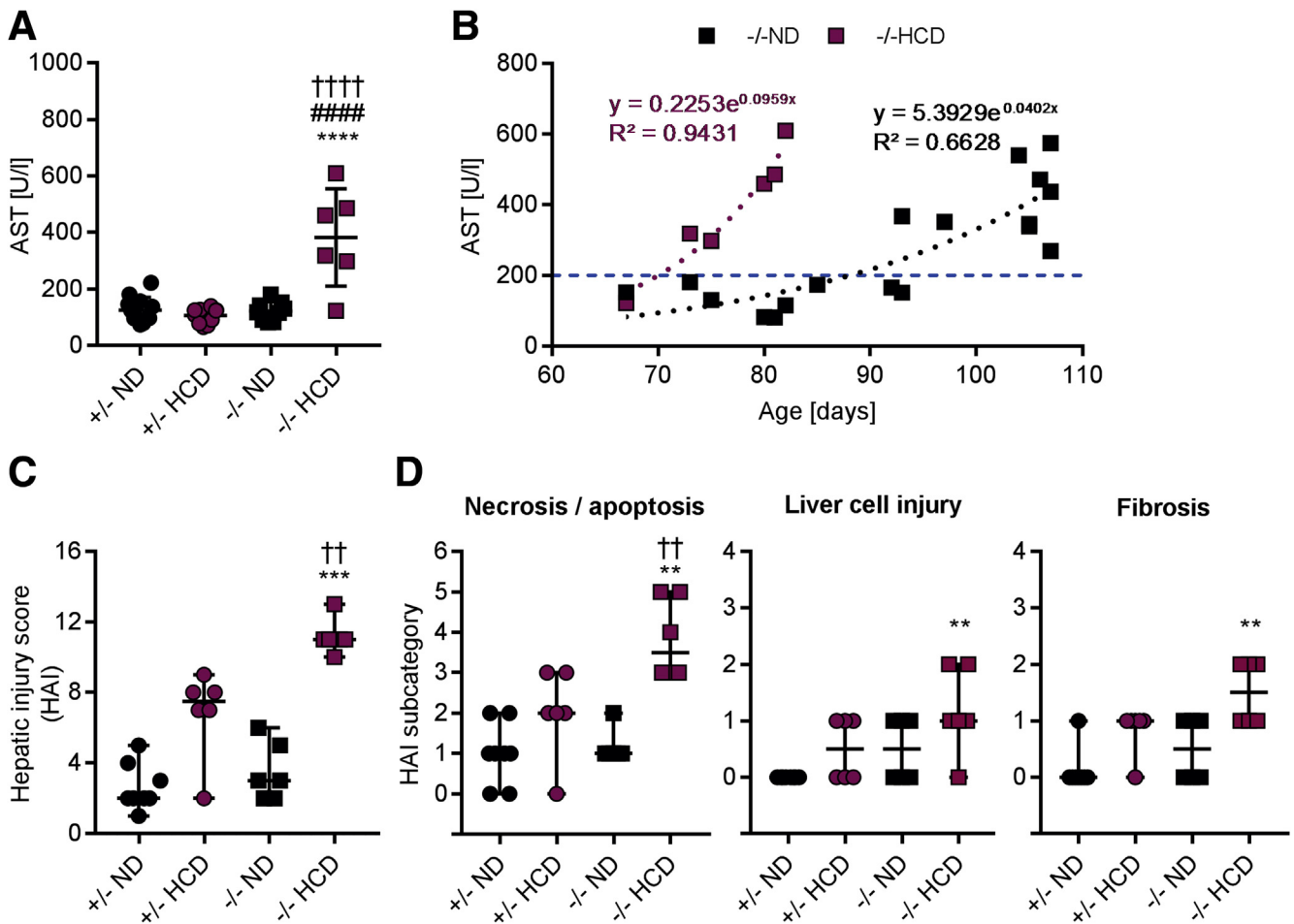


**Figure 2. An HCD causes severe liver damage in *Atp7b*<sup>-/-</sup> rats.** (A) Serum AST is increased specifically in HCD-fed *Atp7b*<sup>-/-</sup> rats (N = 6–12). (B) After disease progression, animals are considered as having clinically apparent WD if AST level is greater than 200 U/L (blue dashed line). HCD causes an earlier disease onset in *Atp7b*<sup>-/-</sup> rats compared with ND-fed animals (HCD, N = 6; ND, N = 18). (C) Total hepatic injury score (HAI, N = 6–8) as well as the (D) HAI score parameters of necrosis, apoptosis, liver cell injury, and fibrosis (N = 6–8) increase significantly only in HCD-fed *Atp7b*<sup>-/-</sup> rats. One-way analysis of variance with the (A) Tukey multiple comparisons test, (B) nonlinear curve fitting, or (C and D) nonparametric Kruskal–Wallis test. N, number of analyzed animals. \*Significant to *Atp7b*<sup>+/-</sup> ND. #Significant to *Atp7b*<sup>+/-</sup> HCD. †Significant to *Atp7b*<sup>-/-</sup> ND. \*,#,†P < .05; \*\*,##,††P < .01; \*\*\*,###,†††P < .001; \*\*\*\*,####,††††P < .0001.

intake (via the HCD) alter hepatic lipid metabolism? To address this question, we subjected liver homogenates of *Atp7b*<sup>+/-</sup> and *Atp7b*<sup>-/-</sup> rats, either ND- or HCD-fed, to a quantitative proteomic comparison (Tables 4–7). This analysis provided evidence for a strongly increased mitochondrial  $\beta$ -oxidation in HCD-fed *Atp7b*<sup>-/-</sup> rats (Table 4). This finding agrees well with our earlier results observed in wild-type mice fed an HCD for a prolonged time, and may be an adaptive response to the increased nutritive fatty acid supply.<sup>13,14</sup> In further agreement, we also observed higher levels of lipid biosynthesis enzymes, partly in HCD-fed *Atp7b*<sup>+/-</sup> control rats, but very prominently in HCD-fed *Atp7b*<sup>-/-</sup> rats (Table 5). In line with these observations, increased triglyceride levels were observed in livers from HCD- vs ND-fed rats (Figure 1B), but not in serum (Figure 6A), and only mildly nonsignificantly increased levels of serum nonesterified free fatty acids (Figure 6B). Thus, the highly increased supply of fatty acids via the HCD

vs ND<sup>14</sup> plausibly causes a 2-fold adaptation in hepatocytes: first, their increased degradation in mitochondria via  $\beta$ -oxidation, and second, their esterification to triglycerides, which preferentially are stored in cytosol.

How would hepatocytes deal with an increasing acetyl coenzyme A (acetyl-CoA) amount resulting from increased mitochondrial  $\beta$ -oxidation of fatty acids? One response is increased lipid biosynthesis and storage. However, acetyl-CoA also is the precursor in hepatic ketogenesis and cholesterol biosynthesis.<sup>32</sup> The proteomic comparison showed only slightly increased to doubled levels of the ketogenic mitochondrial enzymes (Table 6), and first analyses of serum levels indicated comparable 3-hydroxybutyrate levels in HCD- vs ND-fed *Atp7b*<sup>-/-</sup> rats ( $3.25 \pm 0.07$  vs  $3.58 \pm 1.23$  mg/dL, respectively), indicating minor effects on ketogenesis. In contrast, approximately 4-fold increased enzyme levels (in comparison with ND-fed control rats) were found for nearly the whole cholesterol biosynthesis pathway (Table 6).

**Table 3.** Histologic Assessment of Hepatic Injury (HAI Score) in Livers of ND- and HCD-Fed *Atp7b*<sup>+/-</sup> and *Atp7b*<sup>-/-</sup> Rats

			Genotype								
			+/-	+/-	+/-	+/-	+/-	+/-	+/-	+/-	
			Chow	ND	ND	ND	ND	ND	ND	ND	
Hepatic injury score			Animal ID	Rat 3	Rat 15	Rat 1	Rat 2	Rat 14	Rat 16	Rat 17	
Steatosis	Location	Zone 3	0	0	0	0	0	0	0	0	
		Zone 1	1								
		Azonal	2								
	Microvesicular steatosis	Panacinar	3								
		Absent	0	0	0	0	0	0	0	0	
		Present	1								
Inflammation	Microgranulomas	Absent	0								
		Present	1	1	1	1	1	1	1	1	
	Large lipogranulomas	Absent	0	0	0	0	0	0	0	0	
		Present	1								
	Portal inflammation	None to minimal	0	0	0	0	0	0	0	0	
		More than minimal	1								
Liver cell injury	Acidophil bodies	None to rare	0	0	0	0	0	0	0	0	
		Many	1								
	Pigmented macrophages	None to rare	0	0	0	0	0	0	0	0	
		Many	1								
	Megamitochondria	None to rare	0	0	0	0	0	0	0	0	
		Many	1								
Necrosis (periportal/ periseptal interface hepatitis)	Piecemeal necrosis	Absent	0		0	0	0	0	0	0	
		Mild	1	1							
	Mild-moderate	Focal, few portal areas	2								
		Focal, most portal areas	3								
	Moderate	Continuous, approximately <50% tracts/septa	4								
		Continuous, approximately >50% tracts/septa	5								
	Severe	Confluent necrosis	Absent	0	0	0	0	0	0	0	0
			Focal confluent necrosis	1							
		Zone 3 necrosis-some areas	2								
		Zone 3 necrosis-most areas	3								
		Zone 3 necrosis+ occasional bridging (p-c)	4								
		Zone 3 necrosis+ multiple bridging (portal-central)	5								
	Lytic necrosis/ apoptosis/ focal inflammation	Panacinar/multiacinar necrosis	No foci	0			0			0	
≤1 foci per 100× field			1	1	1	1				1	
2-4 foci per 100× field			2					2			
5-10 foci per 100× field			3								
		>10 foci per 200× field	4								
Fibrosis	Stage	None	0	0	0	0	0		0	0	
		Perisinusoidal or periportal	1					1			
		Mild, zone 3	1A								
		Moderate, zone 3	1B								
		Portal/periportal	1C								
		Perisinusoidal and periportal	2								
		Bridging fibrosis	3								
		Cirrhosis	4								
Other findings	Mallory's hyaline	None to rare	0	0	0	0	0		0	0	
		Many	1					1			
		<b>Total</b>		<b>4</b>	<b>2</b>	<b>3</b>	<b>1</b>	<b>5</b>	<b>2</b>	<b>2</b>	

Moreover, in HCD-fed *Atp7b*<sup>-/-</sup> rats, strong increases were found in enzymes responsible for cholesterol excretion via bile acid biosynthesis and bile excretion (Table 7). These data indicated an increased synthesis of cholesterol and plausibly, consequently elevated bile salts in HCD-fed *Atp7b*<sup>-/-</sup> rats. In fact, although unchanged cholesterol levels were determined in serum (Figure 6C) of HCD- vs ND-fed rats, significantly increased bile salt levels were determined only in HCD-fed *Atp7b*<sup>-/-</sup> rat serum (Figure 6D).

### *The High-Affinity Copper Binding Peptide MB Efficiently Reverses HCD-Induced Mitochondrial Dysfunction and Improves Liver Integrity in Atp7b*<sup>-/-</sup> Rats

The bacteria-derived peptide MB prevents disease progression in *Atp7b*<sup>-/-</sup> rats.<sup>4,5</sup> This therapeutic effect is largely owing to efficient hepatic de-coppering (Figure 7A), most prominently in the mitochondrial compartment restoring



**Table 3.** Continued

+/-	+/-	+/-	+/-	+/-	+/-	+/-	-/-	-/-	-/-	-/-	-/-	-/-	-/-	-/-	-/-	-/-	-/-	-/-
ND	HCD	HCD	HCD	HCD	HCD	HCD	ND	ND	ND	ND	ND	ND	HCD	HCD	HCD	HCD	HCD	HCD
Rat 20	Rat 5	Rat 4	Rat 6	Rat 24	Rat 23	Rat 27	Rat 31	Rat 8	Rat 7	Rat 9	Rat 29	Rat 30	Rat 11	Rat 10	Rat 12	Rat 35	Rat 36	Rat 37
0	0	1	0	1	1	2	0	0	0	0	0	0	1	1	2	2	2	2
0	0	1	0	1	1	1	0	0	0	0	0	0	1	1	0	1	1	0
1	1	1	1	1	1	1	1	1	1	1	1	1	1	1	1	1	1	1
0	0	0	0	0	0	0	0	0	0	0	0	0	0	0	0	0	0	0
0	1	1	1	0	1	0	0	1	0	0	0	0	1	1	1	0	0	0
0	0	0	1	1	0	1	0	1	1	1	0	0	1	1	1	1	1	0
0	0	0	0	0	0	0	0	0	0	0	0	0	0	1	1	0	0	0
0	0	0	0	0	0	0	0	0	0	0	0	0	0	0	0	0	0	0
0	0	0	1	1	0	1	0	1	0	0	0	0	1	1	1	1	2	2
0	0	0	0	0	0	0	0	0	0	0	0	0	0	0	0	0	0	0
1	0	2	2	2	2	1	1	1	1	1	1	1	3	2	2	2	3	3
0	0	1	1	1	1	0	1	1	0	0	0	0	1	1	1			
		1									1					2	2	2
0	0	0	1	1	0	0	0	0	0	0	0	0	0	1	1	1	1	1
2	2	7	8	9	7	8	2	6	5	3	3	2	10	11	11	11	13	11

their structure and function.<sup>4,5</sup> Because we aimed here to improve the mitochondrial status in HCD-fed *Atp7b*<sup>-/-</sup> rats as fast as possible, together with a low stress level due to therapy, we chose a once-daily treatment for 5 consecutive days only. We previously observed that such short-term treatments already resulted in mitochondrial improvement, whereas more intense treatments were needed to rescue diseased animals.<sup>5</sup> Consequently, we assessed here

whether the beneficial effect of MB treatment still would hold in HCD-fed *Atp7b*<sup>-/-</sup> rats. Animals were treated once daily for 5 consecutive days with MB, starting at day 75 (ie, at an age when HCD-fed *Atp7b*<sup>-/-</sup> rats presented with marked liver damage) (Figure 2A and B).

MB treatment clearly improved the mitochondrial structure, as evidenced either in situ or at the level of isolated mitochondria (Figure 7B). A significantly lower

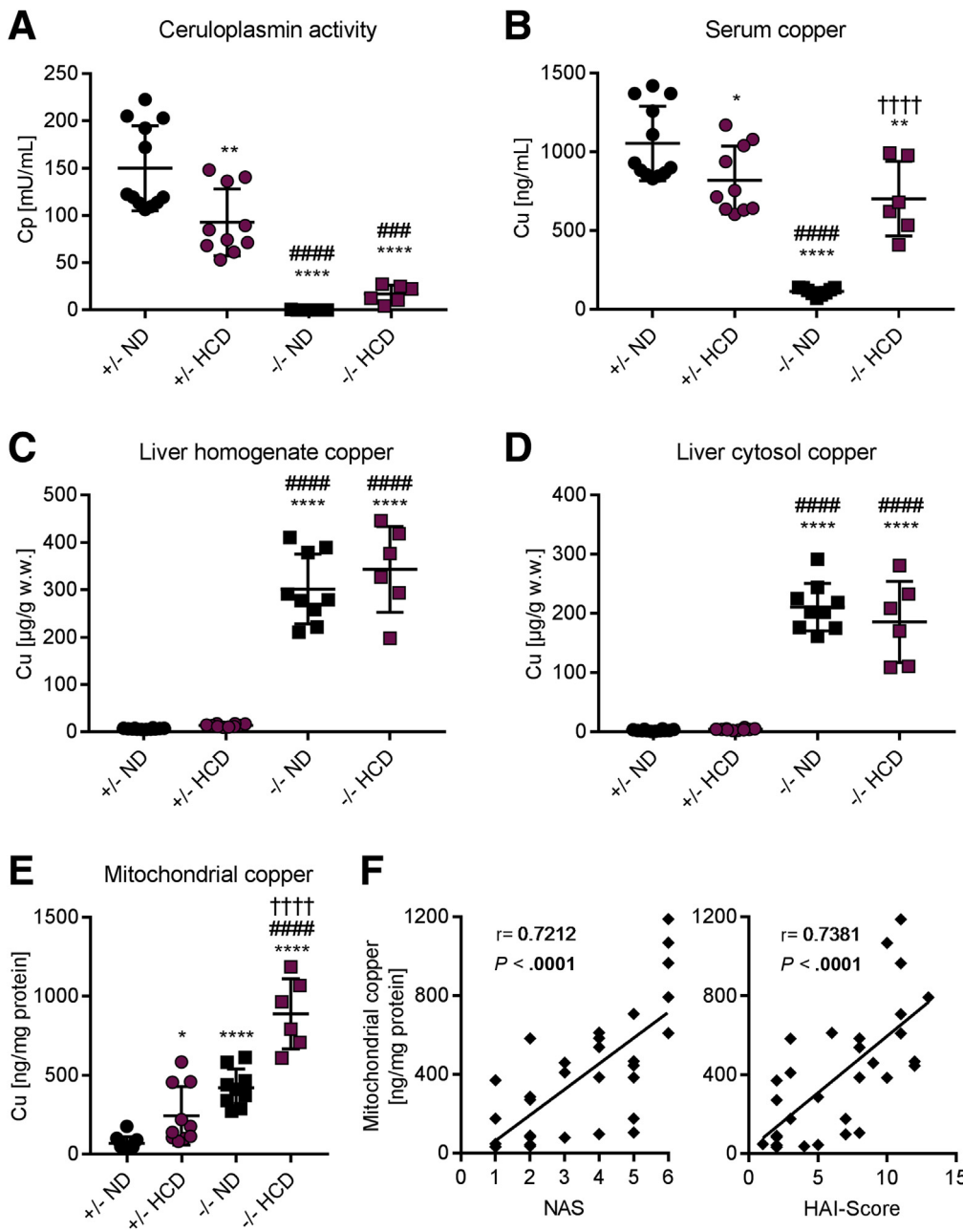


**Figure 3.** An HCD increases the serum and mitochondrial copper load in *Atp7b*<sup>-/-</sup> rats. (A) Serum Cp activity is depleted in *Atp7b*<sup>-/-</sup> rats. (B) Serum copper is decreased in *Atp7b*<sup>-/-</sup> rats compared with *Atp7b*<sup>+/-</sup> rats, but increases upon HCD in *Atp7b*<sup>-/-</sup> rats. (C and D) Equally increased copper load in (C) whole-liver homogenate and (D) hepatic cytosol in either HCD- or ND-fed *Atp7b*<sup>-/-</sup> rats. (E) Massive mitochondrial copper load in HCD-fed *Atp7b*<sup>-/-</sup> rats. (F) The mitochondrial copper load significantly correlates with NAS and HAI score (N = 31). One-way analysis of variance with the (A–E) Tukey multiple comparisons test (N = 6–12), or (F) Spearman correlation. \*Significant to *Atp7b*<sup>+/-</sup> ND. #Significant to *Atp7b*<sup>+/-</sup> HCD. †Significant to *Atp7b*<sup>-/-</sup> ND. \*,#†P < .05; \*\*,#,††P < .01; \*\*\*,###,†††P < .001; \*\*\*\*,####,††††P < .0001. Cu, copper.

number of isolated mitochondria from MB-treated HCD-fed *Atp7b*<sup>-/-</sup> rats presented with cristae detachments and matrix condensations in comparison with mitochondria from untreated HCD-fed *Atp7b*<sup>-/-</sup> rats (Figure 7B, and quantification shown in 7C). This structural normalization was paralleled by a 50% reduction in mitochondrial copper load (Figure 7D, Table 8), highly comparable with our previous results for this treatment regimen (ie, 32%–62% mitochondrial copper depletion using 5 single consecutive MB injections).<sup>5</sup> Moreover, strongly enforced mitochondrial ATP production capacity (Figure 7E) and significantly decreased mitochondrial H<sub>2</sub>O<sub>2</sub> emergence was observed (Figure 7F). Thus, a 5-day-only MB treatment efficiently ameliorated

copper-induced structural and functional deficits in liver mitochondria from HCD-fed *Atp7b*<sup>-/-</sup> rats.

Besides the mitochondrial status, we next investigated effects on overt liver damage upon treatment. All animals experienced a significant decrease in AST serum levels after the MB treatment vs pretreatment levels (Figure 8A, Table 8). One animal that additionally showed increased serum bilirubin levels before treatment returned to levels below the detection limit, and all animals regained weight, showing a positive therapeutic effect (Table 8). In addition, if compared with untreated HCD-fed *Atp7b*<sup>-/-</sup> rats, we found significantly lower serum copper levels and a massive decrease in total serum bile salts (Figure 8B and C). Thus,

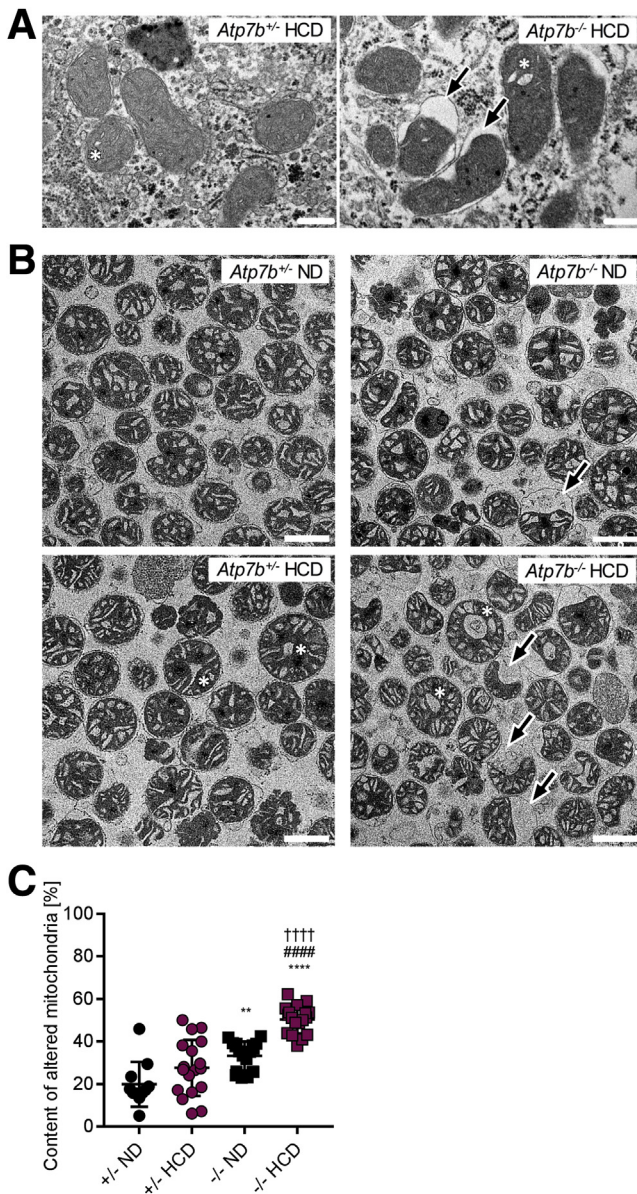


**Figure 4. An HCD amplifies hepatic mitochondrial damage in WD *Atp7b*<sup>-/-</sup> rats.** (A and B) Mitochondria either (A) in situ (scale bar: 250 nm) or (B) isolated (scale bar: 1  $\mu$ m) from HCD-fed *Atp7b*<sup>-/-</sup> rats presenting with severe structural alterations, including detachments of the mitochondrial inner and outer membranes (arrows) or matrix condensations together with ballooned cristae (asterisk). (C) Quantification of structurally altered mitochondria from the 4 animal groups. One-way analysis of variance with the Tukey multiple comparisons test (N = 2–3, 350–750 mitochondria per group of animal). \*Significant to *Atp7b*<sup>+/-</sup> ND. #Significant to *Atp7b*<sup>+/-</sup> HCD. †Significant to *Atp7b*<sup>-/-</sup> ND. \*,#†P < .05; \*\*,##,††P < .01; \*\*\*,###,†††P < .001; \*\*\*\*,####,††††P < .0001.

overt liver damage was rescued by this short-term MB treatment. At a histologic level, however, liver damage of HCD-fed *Atp7b*<sup>-/-</sup> rats only partially was resolved (Figures 8D–F), resulting in a mild but significant decrease in NAS (Figures 8F), while liver triglyceride levels were unchanged (Figure 8G).

## Discussion

In WD, ATP7B malfunction impairs hepatic copper excretion. This leads to a progressive copper burden in mitochondria.<sup>4,5,8,30</sup> Copper ultimately causes mitochondrial destruction, hepatocyte death, liver failure, and decease of WD *Atp7b*<sup>-/-</sup> rats.<sup>5</sup> We previously reported that efficient depletion of mitochondrial copper load with the high-affinity copper chelator MB leads to full recovery from even severe states of liver damage.<sup>5</sup> Upon pausing still, the rate of mitochondrial copper re-accumulation determines the rate of re-occurring liver damage.<sup>5</sup>

These findings show that hepatic mitochondria are exceptionally susceptible to liver copper overload, thereby being a key organelle in WD pathogenesis. However, mitochondria also readily respond to environmental changes other than increased copper by metabolic adaptations and can balance imposed challenges to different extents for a long time.<sup>13,33</sup> We reasoned that this mitochondrial flexibility might contribute to the high variability of the clinical presentation of WD.<sup>1</sup> The *ATP7B* genotype is not clearly predictive for the age of onset, the disease presentation or progression, or for the response to treatment.<sup>1,34</sup> This absence of a genotype–phenotype correlation may be best exemplified by studies on genetically identical WD twins, whose clinical appearance ranged from presymptomatic phenotypes to liver failure.<sup>17,35</sup> Consequently, it has been suggested that the WD phenotype may be highly attributable to environmental factors.<sup>35,36</sup>

Steatosis is a frequently observed early characteristic in livers of WD patients,<sup>8,9</sup> and mutations in the  $\epsilon 3$  and  $\epsilon 4$  isoforms of the apolipoprotein E gene are associated with WD onset.<sup>37,38</sup> Moreover, mutations in the lipase gene *PNALP3* are linked to the percentage of liver steatosis in patients with WD.<sup>9</sup> Furthermore, lower serum cholesterol levels were observed in WD patients with hepatic symptoms,<sup>39,40</sup> and WD animal models, such as *Atp7b*<sup>-/-</sup> mice, present a down-regulation of enzymes involved in cholesterol and lipid metabolism,<sup>22,41</sup> whereas Long-Evans Cinnamon rats show lower serum but higher liver cholesterol and triglyceride levels.<sup>21</sup> These studies clearly indicate a link between the lipid/cholesterol metabolism and WD pathophysiology. We therefore asked whether a steatosis-promoting diet would influence WD-related liver damage, and especially mitochondrial damage, in *Atp7b*<sup>-/-</sup> rats. The rationale was that both enriched copper and fatty acids cause bioenergetic defects and therefore synergistically and detrimentally may coincide on hepatic mitochondria.

An HCD caused strongly increased and accelerated liver damage, evidenced by serum markers of liver damage (Figure 2A and B) and histologic assessment (HAI score and NAS). In HCD- vs ND-fed *Atp7b*<sup>-/-</sup> rats, a drastically increased copper load was found in mitochondria, but equal cytosolic or overall hepatic copper contents. Compared with mitochondria from either HCD- or ND-fed control rats or from ND-fed *Atp7b*<sup>-/-</sup> rats, mitochondria from HCD-fed *Atp7b*<sup>-/-</sup> rats appeared to have the most severe mitochondrial structural alterations, a significantly lower ATP production, and a significantly enhanced mitochondrial ROS emergence.

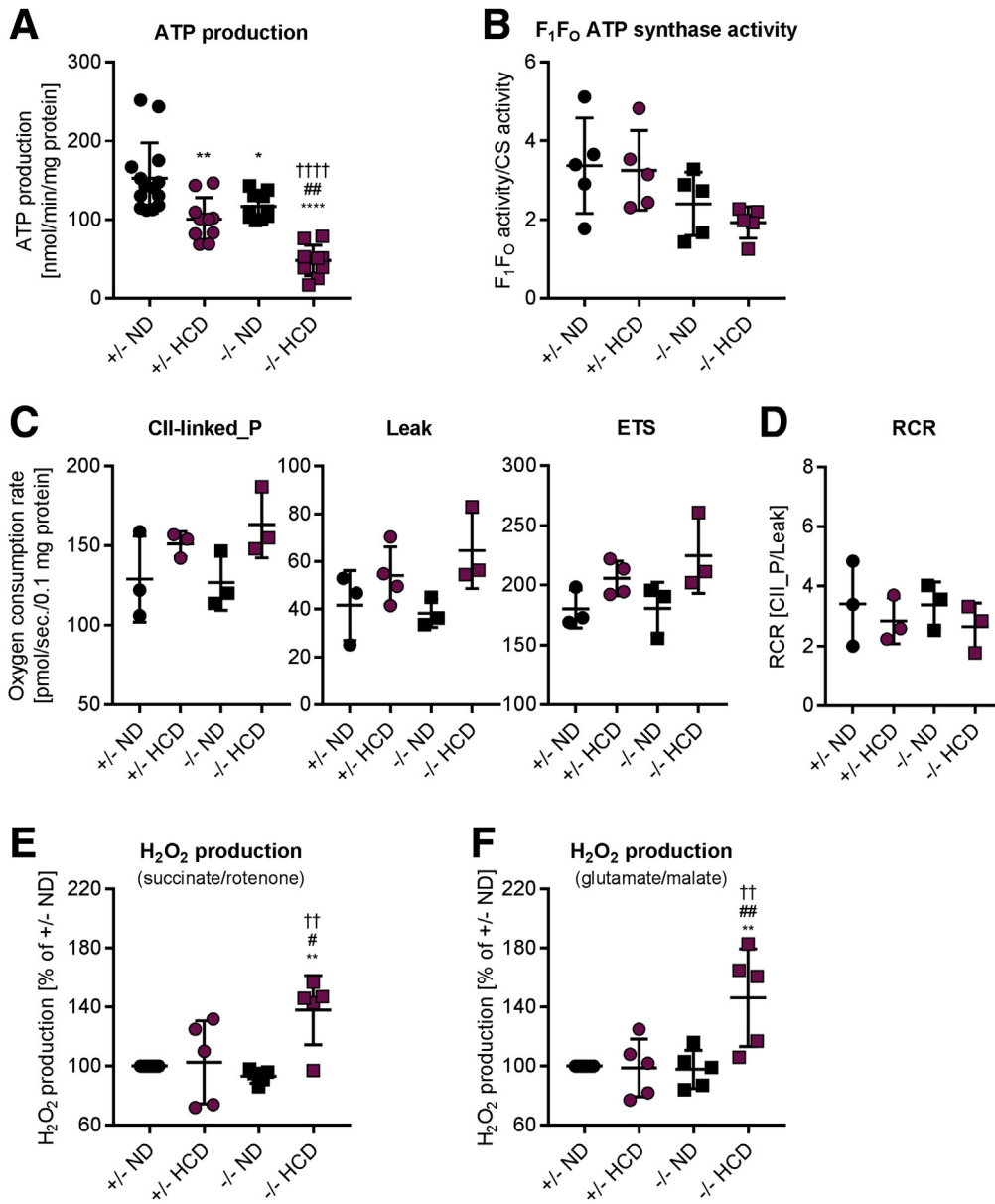


**Figure 5. An HCD severely impairs mitochondrial function in *Atp7b*<sup>-/-</sup> rats.** (A) HCD feeding significantly reduces mitochondrial ATP production capacity in *Atp7b*<sup>-/-</sup> rats (N = 5–7). (B) Tendentiously lowest F<sub>1</sub>F<sub>0</sub> activity (ATP synthase, normalized to CS activity) in mitochondria from HCD-fed *Atp7b*<sup>-/-</sup> rats (N = 5). HCD feeding (C) hardly affected mitochondrial oxygen consumption and (D) did not change respiratory control ratios (RCR; N = 3). (E and F) Strongly increased H<sub>2</sub>O<sub>2</sub> emergence from mitochondria of HCD-fed *Atp7b*<sup>-/-</sup> rats using either (E) succinate/rotenone and ADP or (F) glutamate/malate as substrates (N = 5). One-way analysis of variance with the Tukey multiple comparisons test. \*Significant to *Atp7b*<sup>+/-</sup> ND. #Significant to *Atp7b*<sup>+/-</sup> HCD. †Significant to *Atp7b*<sup>-/-</sup> ND. \*,#†P < .05; \*\*,##,††P < .01; \*\*\*,###,†††P < .001; \*\*\*\*,####,††††P < .0001. CII-linked\_P, succinate-linked phosphorylation; LEAK, oxygen consumption upon oligomycin treatment; ETS, electron transfer system capacity in a noncoupled carbonyl cyanide-4-(trifluoromethoxy) phenylhydrazone (FCCP)-treated state.

Hence, the combination of an HCD with an increasing copper load caused severe structural and functional mitochondrial impairments, whereas mitochondrial copper overload strongly correlated with progressive liver damage (Figures 2–5).

Thus, a simple change in nutrition from a normal diet to an HCD severely aggravated and accelerated WD pathophysiology in HCD-fed *Atp7b*<sup>-/-</sup> rats. This could be the result of 2 not mutually exclusive reasons: enhanced copper uptake and/or an additional metabolic burden imposed on the hepatocytes and their mitochondria because the latter organelles are both the prime site for cellular copper utilization (via complex IV of the respiratory chain) and for fatty acid degradation. Based on reports that ND-fed control animals consumed similar amounts of food and water as their HCD-fed counterparts,<sup>24</sup> we adjusted for an equal copper

supply by the 2 diets (see the Materials and Methods section). In subsequent testing, however, we found that the rats consumed less HCD than ND food, but more fructose water instead of water, respectively. Upon recalculating the supplied copper amounts, we found that the HCD/syrup diet provided approximately 18% more copper. Interestingly, this slightly increased copper supply, however, did not result in correspondingly increased liver copper levels (Figure 3) because we observed equal copper loads in total liver homogenates and in liver cytosol. To the contrary, mitochondria from HCD- vs ND-fed control animals had drastically and significantly increased copper levels (Figure 3). This may indicate that the distribution of hepatocyte copper changes upon HCD feeding. In the HCD-fed *Atp7b*<sup>-/-</sup> rat liver mitochondria this copper overload caused severe structural and functional mitochondrial



**Table 4.** Quantitative Proteome Comparisons of Liver Homogenate Proteins of the  $-/-$  ND,  $+/-$  HCD, and  $-/-$  HCD Groups Vs  $+/-$  ND Group: Fatty Acid Degradation ( $\beta$ -Oxidation)

Symbol	Description	$-/-$ ND vs $+/-$ ND	$+/-$ HCD vs $+/-$ ND	$-/-$ HCD vs $+/-$ ND	Cellular localization
Acot13	Acyl-CoA thioesterase 13	0.87	1.12	3.12 <sup>a</sup>	Mitochondrion
Echdc2	Enoyl-CoA hydratase domain containing 2	1.08	1.00	2.39 <sup>a</sup>	Mitochondrion
Echdc3	Enoyl-CoA hydratase domain containing 3	1.15	0.90	2.11 <sup>a</sup>	Mitochondrion
Etfdh	Electron-transferring-flavoprotein dehydrogenase	1.16	0.84	2.09 <sup>a</sup>	Mitochondrion
Ivd	Isovaleryl-CoA dehydrogenase	1.26	1.33	3.03 <sup>a</sup>	Mitochondrion
Mcee	Methylmalonyl CoA epimerase	0.94	1.14	2.68 <sup>a</sup>	Mitochondrion
Acad5b	Acyl-CoA dehydrogenase, short/branched chain	0.93	1.73 <sup>b</sup>	1.90 <sup>b</sup>	Mitochondrion
Decr1	2,4-Dienoyl CoA reductase 1, mitochondrial	0.99	0.60 <sup>b</sup>	1.52 <sup>b</sup>	Mitochondrion
Acaa2	Acetyl-CoA acyltransferase 2	0.99	0.93	1.65 <sup>b</sup>	Mitochondrion
Acads	Acyl-CoA dehydrogenase, C-2 to C-3 short chain	0.99	0.95	1.56 <sup>b</sup>	Mitochondrion
Auh	Adenosine-uridine RNA binding protein/enoyl-CoA hydratase	1.09	1.03	1.58 <sup>b</sup>	Mitochondrion
Echs1	Enoyl-CoA hydratase, short chain, 1, mitochondrial	0.90	1.28	2.00 <sup>b</sup>	Mitochondrion
Etf $\alpha$	Electron-transfer-flavoprotein, $\alpha$ polypeptide	0.98	1.13	1.98 <sup>b</sup>	Mitochondrion
Etf $\beta$	Electron-transfer-flavoprotein, $\beta$ polypeptide	1.08	1.21	1.79 <sup>b</sup>	Mitochondrion
Gcdh	Glutaryl-CoA dehydrogenase	0.86	1.09	1.91 <sup>b</sup>	Mitochondrion
Hacl1	2-Hydroxyacyl-CoA lyase 1	1.24	0.75	1.92 <sup>b</sup>	Mitochondrion
Hadh	Hydroxyacyl-CoA dehydrogenase	0.96	0.75	1.81 <sup>b</sup>	Mitochondrion
Mut	Methylmalonyl CoA mutase	1.09	1.29	1.67 <sup>b</sup>	Mitochondrion
Pcca	Propionyl-CoA carboxylase, $\alpha$ polypeptide	1.08	1.19	1.81 <sup>b</sup>	Mitochondrion
Pccb	Propionyl-CoA carboxylase, $\beta$ polypeptide	1.00	1.11	1.96 <sup>b</sup>	Mitochondrion
Acot2	Acyl-CoA thioesterase 2	1.10	0.40 <sup>a</sup>	0.65 <sup>b</sup>	Mitochondrion
Acad9	Acyl-CoA dehydrogenase family, member 9	0.76	0.96	0.63 <sup>b</sup>	Mitochondrion
Mmaa	Methylmalonic aciduria (cobalamin deficiency) cblA type	1.10	1.33	0.55 <sup>b</sup>	Mitochondrion
Eci1	Enoyl-CoA delta isomerase 1	0.89	0.50 <sup>b</sup>	0.70	Mitochondrion
Ehhadh	Enoyl-CoA, hydratase/3-hydroxyacyl CoA dehydrogenase	1.20	0.65 <sup>b</sup>	0.99	Mitochondrion
Hadha	Hydroxyacyl-CoA dehydrogenase/3-ketoacyl-CoA thiolase/enoyl-CoA hydratase (trifunctional protein), $\alpha$ subunit	0.86	0.62 <sup>b</sup>	1.07	Mitochondrion
Acad10	Acyl-CoA dehydrogenase family, member 10	0.86	0.90	1.30	Mitochondrion
Acad11	Acyl-CoA dehydrogenase family, member 11	0.91	0.90	0.75	Mitochondrion
Acad8	Acyl-CoA dehydrogenase family, member 8	0.97	1.26	1.02	Mitochondrion
Acadl	Acyl-CoA dehydrogenase, long chain	1.07	0.79	1.26	Mitochondrion
Acadm	Acyl-CoA dehydrogenase, C-4 to C-12 straight chain	0.95	1.04	0.99	Mitochondrion
Acadvl	Acyl-CoA dehydrogenase, very long chain	0.87	0.72	0.98	Mitochondrion
Cpt1a	Carnitine palmitoyltransferase 1a, liver	1.10	0.68	0.94	Mitochondrion
Cpt2	Carnitine palmitoyltransferase 2	0.87	0.81	1.01	Mitochondrion
Mcat	Malonyl-CoA-acyl carrier protein transacylase (mitochondrial)	0.71	0.74	1.12	Mitochondrion
Mecr	Mitochondrial trans-2-enoyl-CoA reductase	0.93	1.06	1.32	Mitochondrion
Acox2	Acyl-CoA oxidase 2, branched chain	1.08	0.83	2.54 <sup>a</sup>	Peroxisome, mitochondrion
Phyh	Phytanoyl-CoA 2-hydroxylase	1.20	1.48	2.39 <sup>a</sup>	Peroxisome, mitochondrion
Abcd3	ATP-binding cassette, subfamily D, member 3	0.95	0.64 <sup>b</sup>	0.77	Peroxisome, mitochondrion
Ech1	Enoyl-CoA hydratase 1, peroxisomal	1.01	0.66 <sup>b</sup>	1.06	Peroxisome, mitochondrion
Acox3	Acyl-CoA oxidase 3, pristanoyl	1.00	0.75	1.12	Peroxisome, mitochondrion
Eci3	Enoyl-CoA delta isomerase 3	0.91	0.91	1.34	Peroxisome, mitochondrion

Table 4. Continued

Symbol	Description	-/- ND vs +/- ND	+/- HCD vs +/- ND	-/- HCD vs +/- ND	Cellular localization
Eci3	Enoyl-CoA delta isomerase 3	0.77	0.91	0.85	Peroxisome, mitochondrion
Slc27a2	Solute carrier family 27 (fatty acid transporter), member 2	1.03	0.82	1.07	ER, mitochondrion
Hac11	2-Hydroxyacyl-CoA lyase 1	1.24	0.75	1.92 <sup>b</sup>	Peroxisome
Acot4	Acyl-CoA thioesterase 4	1.10	0.48 <sup>a</sup>	0.44 <sup>a</sup>	Peroxisome
Acot8	Acyl-CoA thioesterase 8	1.05	0.91	0.49 <sup>a</sup>	Peroxisome, cytoplasm
Acox1	Acyl-CoA oxidase 1, palmitoyl	1.09	0.62 <sup>b</sup>	1.17	Peroxisome
Acaa1a	Acetyl-CoA acyltransferase 1	1.01	1.00	0.82	Peroxisome
Acot12	Acyl-CoA thioesterase 12	1.04	0.86	0.99	Cytoplasm
Acox1	Acyl-CoA oxidase 1, palmitoyl	0.87	0.81	1.49	Peroxisome
Decr2	2,4-dienoyl CoA reductase 2, peroxisomal	1.08	0.80	0.84	Peroxisome
Hadhb	Hydroxyacyl-CoA dehydrogenase/3-ketoacyl-CoA thiolase/enoyl-CoA hydratase (trifunctional protein), β subunit	0.92	0.71	0.97	Peroxisome
Hsd17b4	Hydroxysteroid (17-β) dehydrogenase 4	1.04	0.85	1.01	Peroxisome

NOTE. Data are presented as mean ratios from 3 age-matched animals (age, 80–82 days).  
ER, endoplasmic reticulum.

<sup>a</sup>Fold-changes greater than 2 compared with +/-ND control.

<sup>b</sup>Fold-changes between 1.5 and 2.0 compared with +/-ND control.

deficits (Figures 4 and 5), paralleled by cell death (Figure 2). We recently reported that progressive mitochondrial copper accumulation causes a steady reduction of their capacity to produce ATP.<sup>5</sup> This is owing to the direct impact of copper on the protein complexes involved in ATP production, but also ATP delivery to the cytosol.<sup>4</sup> This bioenergetic deficit matches the clinical presentation of liver damage in *Atp7b*<sup>-/-</sup> rats. A decrease in the ATP production capacity to 70% in comparison with mitochondria from *Atp7b*<sup>+/-</sup> control rats was found to be critical for the onset of clinically apparent liver damage (ie, AST levels > 200 U/L).<sup>5</sup> In the present study, a mitochondrial ATP production capacity of 80% was preserved in young ND-fed *Atp7b*<sup>-/-</sup> rats (Figure 5A). In agreement with our earlier study, these rats still were healthy (Figure 2). In a mouse study, we reported that the increased supply of fatty acids via an HCD causes lipidomic alterations in the membranes of liver mitochondria that also reduce their ATP production capacity,<sup>13</sup> along with only mild signs of liver impairment.<sup>13</sup> In agreement with this study, we determined a reduced mitochondrial ATP production capacity but comparatively mild signs of apparent liver damage in HCD-fed *Atp7b*<sup>+/-</sup> control vs *Atp7b*<sup>-/-</sup> rats (steatohepatitis was present in only 2 of 6 HCD-fed *Atp7b*<sup>+/-</sup> rats) (Figures 1C, 2, and 5A, Tables 1 and 3). This situation changed when an increasing copper load coincided with steatosis: a decreased ATP production capacity to less than 40% was paralleled by severe structural impairments and strongly increased ROS emergence in mitochondria from HCD-fed *Atp7b*<sup>-/-</sup> rats, in comparison with mitochondria from all other rats, whether HCD- or ND-fed controls or ND-fed *Atp7b*<sup>-/-</sup> rats (Figures 4 and 5). One interesting question for future experiments is why mitochondrial turnover and

renewal via mitophagy was incapable to rescue the detrimental effects of copper and steatosis coinciding on mitochondria. Either such pathways were efficiently inactivated (possibly involving activated mechanistic target of rapamycin (mTOR) pathways), blocked by copper excess, negatively affected by bioenergetic deficits that were too strong, or simply overwhelmed. As a result, however, such mitochondrial damage strongly challenges hepatocytes, and cell death (both necrosis and apoptosis) was extensive (Figure 2D), paralleled by severe liver damage in HCD-fed *Atp7b*<sup>-/-</sup> rats (Figure 2, Tables 1–3). We therefore conclude that WD pathophysiology in HCD-fed *Atp7b*<sup>-/-</sup> rats is aggravated because of a highly detrimental combination of massive copper- and fatty acid-induced impacts on liver mitochondria.

Further support for the decisive role of mitochondrial damage in the pathophysiology of HCD-fed *Atp7b*<sup>-/-</sup> rats comes from the results of the applied short-term treatment with the copper chelator MB (Figures 7 and 8). We chose this drug, and applied it once daily for 5 consecutive days, to test for a fast mitochondrial recovery in HCD-fed *Atp7b*<sup>-/-</sup> rats, as a potential remedy against acute and overt liver damage. In comparison with our earlier reports, such treatments are relatively mild because we also had applied MB 2 or 3 times daily or for increased time periods of up to 1 month.<sup>4,5</sup> Nevertheless, this short-term MB treatment significantly reduced mitochondrial structural damage and improved mitochondrial ATP production with a concomitant decrease in ROS emergence (Figure 7). This mitochondrial amelioration was paralleled by a rescue of overt/acute liver damage in all treated animals, as serum AST levels decreased, bilirubin levels were below detection and

**Table 5.** Quantitative Proteome Comparisons of Liver Homogenate Proteins of the  $-/-$  ND,  $+/-$  HCD, and  $-/-$  HCD Groups Vs  $+/-$  ND Group: Fatty Acid and Triglyceride Synthesis

Symbol	Description	$-/-$ ND vs $+/-$ ND	$+/-$ HCD vs $+/-$ ND	$-/-$ HCD vs $+/-$ ND	Cellular localization
<b>Fatty acid synthesis</b>					
Acsm3	Acyl-CoA synthetase medium-chain family member 3	0.84	2.79 <sup>a</sup>	4.25 <sup>a</sup>	Mitochondrion
Acss2	Acyl-CoA synthetase short-chain family member 2	1.22	1.56 <sup>b</sup>	2.09 <sup>a</sup>	Cytoplasm, nucleus
Elovl5	Elongation of very long chain fatty acids protein 5	1.64 <sup>b</sup>	0.89	2.12 <sup>a</sup>	ER
Tecr	Trans-2,3-enoyl-CoA reductase	1.42	1.01	2.85 <sup>a</sup>	ER
Acs1	Acyl-CoA synthetase long-chain family member 1	1.14	0.83	3.46 <sup>a</sup>	ER, mitochondrion
Acsm1	Acyl-CoA synthetase medium-chain family member 1	0.92	1.06	2.35 <sup>a</sup>	Mitochondrion
Acss3	Acyl-CoA synthetase short-chain family member 3	0.90	1.26	2.39 <sup>a</sup>	Mitochondrion
Fads2	Fatty acid desaturase 2	0.87	3.25 <sup>a</sup>	1.62 <sup>b</sup>	ER
Hsd17b8	Hydroxysteroid (17- $\beta$ ) dehydrogenase 8	0.95	0.98	1.83 <sup>b</sup>	Mitochondrion
LOC683884	Similar to acyl carrier protein, mitochondrial precursor	1.16	1.03	1.52 <sup>b</sup>	Mitochondrion
Acacb	Acetyl-CoA carboxylase $\beta$	1.30	1.37	1.89 <sup>b</sup>	Mitochondrion, nucleus
Pecr	Peroxisomal trans-2-enoyl-CoA reductase	0.98	0.97	1.77 <sup>b</sup>	Peroxisome, mitochondrion
Acsm1	Acyl-CoA synthetase medium-chain family member 1	0.67	3.43 <sup>a</sup>	0.18 <sup>a</sup>	Mitochondrion
Acsf2	Acyl-CoA synthetase family member 2	0.68	1.66 <sup>b</sup>	0.56 <sup>b</sup>	Mitochondrion
Acsm5	Acyl-CoA synthetase medium-chain family member 5	0.59 <sup>b</sup>	0.56 <sup>b</sup>	0.53 <sup>b</sup>	Mitochondrion
Fasn	Fatty acid synthase	1.08	0.26 <sup>a</sup>	0.77	Cytoplasm
Acly	ATP citrate lyase	1.06	0.34 <sup>a</sup>	0.97	Nucleus
Acaca	Acetyl-CoA carboxylase $\alpha$	1.18	0.55 <sup>b</sup>	0.83	Mitochondrion
Acs14	Acyl-CoA synthetase long-chain family member 4	1.17	0.65 <sup>b</sup>	1.29	Mitochondrion
Hacd2	3-hydroxyacyl-CoA dehydratase 2	1.00	1.31	1.45	ER
Hsd17b12	Hydroxysteroid (17- $\beta$ ) dehydrogenase 12	1.03	0.88	1.11	ER
Hacd3	3-hydroxyacyl-CoA dehydratase 3	1.32	1.16	1.10	ER, mitochondrion
Ppt1	Palmitoyl-protein thioesterase 1	1.05	1.06	0.81	Lysosome
Acsf3	Acyl-CoA synthetase family member 3	0.93	1.22	1.03	Mitochondrion
Acs15	Acyl-CoA synthetase long-chain family member 5	1.27	0.68	1.16	Mitochondrion
Cbr4	Carbonyl reductase 4	0.89	0.83	1.04	Mitochondrion
Mcat	Malonyl-CoA-acyl carrier protein transacylase	0.71	0.74	1.12	Mitochondrion
Mecr	Mitochondrial trans-2-enoyl-CoA reductase	0.93	1.06	1.32	Mitochondrion
Slc25a1	Solute carrier family 25 (mitochondrial carrier, citrate transporter), member 1	1.20	1.03	1.30	Mitochondrion
<b>Triglyceride synthesis</b>					
Gk	Glycerol kinase	1.30	0.75	2.16 <sup>a</sup>	Mitochondrion
Gpam	Glycerol-3-phosphate acyltransferase	1.16	0.94	1.97 <sup>b</sup>	Mitochondrion
Agmo	Alkylglycerol monooxygenase	0.82	0.69	0.75	ER
Dgat1	Diacylglycerol O-acyltransferase 1	1.09	1.13	1.24	ER

NOTE. Data are presented as mean ratios from 3 age-matched animals (age, 80–82 days). ER, endoplasmic reticulum.

<sup>a</sup>Fold-changes greater than 2 compared with  $+/-$ ND control.

<sup>b</sup>Fold-changes between 1.5 and 2.0 compared with  $+/-$ ND control.

animals regained body weight (Table 8). In addition, compared with untreated HCD-fed *Atp7b*<sup>-/-</sup> rats, serum copper and bile salt levels, plausibly increased upon hepatocyte disintegration, significantly decreased in MB-treated HCD-fed *Atp7b*<sup>-/-</sup> rats (Figure 8B and C).

Despite this highly beneficial effect of the applied short-term MB-treatment, mitochondrial and liver rescue was not complete. Although the mitochondrial copper content decreased to 50% (Figure 7D), in absolute terms, the remaining copper load still was a borderline burden

**Table 6.** Quantitative Proteome Comparisons of Liver Homogenate Proteins of the  $-/-$  ND,  $+/-$  HCD, and  $-/-$  HCD Groups Vs  $+/-$  ND Group: Ketone Body and Cholesterol Synthesis

Symbol	Description	$-/-$ ND vs $+/-$ ND	$+/-$ HCD vs $+/-$ ND	$-/-$ HCD vs $+/-$ ND	Cellular localization
<b>Ketone body synthesis</b>					
Acss3	Acyl-CoA synthetase short-chain family member 3	0.90	1.26	2.39 <sup>a</sup>	Mitochondrion
Bdh1	3-Hydroxybutyrate dehydrogenase, type 1	0.95	0.82	3.20 <sup>a</sup>	Mitochondrion
Hmgcs2	3-Hydroxy-3-methylglutaryl-CoA synthase 2	1.04	0.58 <sup>b</sup>	1.95 <sup>b</sup>	Mitochondrion
Acat1	Acetyl-CoA acetyltransferase 1	0.92	0.82	1.30	Mitochondrion
Hmgcl	3-Hydroxymethyl-3-methylglutaryl-CoA lyase	0.81	0.87	1.43	Mitochondrion
<b>Cholesterol synthesis</b>					
Acat2	Acetyl-CoA acetyltransferase 2	1.73 <sup>b</sup>	2.67 <sup>a</sup>	8.79 <sup>a</sup>	Nucleus
Hsd17b7	Hydroxysteroid (17- $\beta$ ) dehydrogenase 7	1.57 <sup>b</sup>	2.03 <sup>a</sup>	6.52 <sup>a</sup>	Cell membrane
Idi1	Isopentenyl-diphosphate delta isomerase 1	1.63 <sup>b</sup>	4.08 <sup>a</sup>	3.39 <sup>a</sup>	Peroxisome
Msmo1	Methylsterol monooxygenase 1	1.70 <sup>b</sup>	3.25 <sup>a</sup>	4.16 <sup>a</sup>	ER
Cyp51	Cytochrome P450, family 51, lanosterol 14- $\alpha$ demethylase	1.31	2.60 <sup>a</sup>	4.75 <sup>a</sup>	Unknown
Hmgcs1	3-Hydroxy-3-methylglutaryl-CoA synthase 1 (soluble)	1.08	2.60 <sup>a</sup>	3.74 <sup>a</sup>	Cytoplasm
Mvk	Mevalonate kinase	1.21	2.21 <sup>a</sup>	4.12 <sup>a</sup>	Peroxisome
Sqle	Squalene epoxidase	1.47	3.62 <sup>a</sup>	4.05 <sup>a</sup>	ER
Ebp	Emopamil binding protein (sterol isomerase)	1.66 <sup>b</sup>	1.68 <sup>b</sup>	2.71 <sup>a</sup>	ER
Dhcr7	7-Dehydrocholesterol reductase	1.37	1.77 <sup>b</sup>	2.42 <sup>a</sup>	ER
Lss	Lanosterol synthase (2,3-oxidosqualene-lanosterol cyclase)	1.40	1.98 <sup>b</sup>	4.01 <sup>a</sup>	ER
Pmvk	Phosphomevalonate kinase	1.22	1.73 <sup>b</sup>	4.47 <sup>a</sup>	Peroxisome
Tm7sf2	Transmembrane 7 superfamily member 2	1.17	1.88 <sup>b</sup>	3.84 <sup>a</sup>	ER
Fdps	Farnesyl diphosphate synthase	1.49	1.30	3.99 <sup>a</sup>	Cytoplasm
Mvd	Mevalonate (diphospho) decarboxylase	1.01	2.00 <sup>a</sup>	1.94 <sup>b</sup>	Peroxisome
Fdft1	Farnesyl diphosphate farnesyl transferase 1	1.22	1.99 <sup>b</sup>	1.80 <sup>b</sup>	ER
Hmgcs2	3-Hydroxy-3-methylglutaryl-CoA synthase 2	1.04	0.58 <sup>b</sup>	1.95 <sup>b</sup>	Mitochondrion
Acaa2	Acetyl-CoA acyltransferase 2	0.99	0.93	1.65 <sup>b</sup>	Mitochondrion
Dhcr24	24-Dehydrocholesterol reductase	1.17	1.87 <sup>b</sup>	1.35	ER, Golgi
Acat1	Acetyl-CoA acetyltransferase 1	0.92	0.82	1.30	Mitochondrion
Hmgcl	3-Hydroxymethyl-3-methylglutaryl-CoA lyase	0.81	0.87	1.43	Mitochondrion
Nsdhl	NAD(P)-dependent steroid dehydrogenase-like	1.06	0.92	1.00	ER

NOTE. Data are presented as mean ratios from 3 age-matched animals (age, 80–82 days). ER, endoplasmic reticulum.

<sup>a</sup>Fold-changes greater than 2 compared with  $+/-$  ND control.

<sup>b</sup>Fold-changes between 1.5 and 2.0 compared with  $+/-$  ND control.

(Table 8) and comparable with the values of ND-fed *Atp7b*<sup>-/-</sup> rats (Figure 3E) that were about to develop hepatitis within days (Figure 2B). This borderline status may explain the noticeable but limited improvements in liver histology (Figure 8), and it remains for future studies to test whether prolonged/intensified MB treatments would result in a more complete reversal of mitochondrial and liver damage in HCD-fed *Atp7b*<sup>-/-</sup> rats.

HCD feeding caused steatosis in all HCD-fed animals. In contrast, steatohepatitis was present in only 2 of 6 HCD-fed *Atp7b*<sup>+/-</sup> rats, but in all 6 HCD-fed *Atp7b*<sup>-/-</sup> rats (Figure 1, Table 1). Accordingly, tendentious lower levels of visceral fat (Figure 1A) and lower levels of liver triglycerides (Figure 1B) were found in HCD-fed *Atp7b*<sup>-/-</sup> vs *Atp7b*<sup>+/-</sup> rats, indicating a comparatively higher energy turnover in *Atp7b*<sup>-/-</sup> livers. Indeed, mitochondrial enzymes involved in



**Table 7.** Quantitative Proteome Comparisons of Liver Homogenate Proteins of the  $-/-$  ND,  $+/-$  HCD, and  $-/-$  HCD Groups Vs  $+/-$  ND Group: Bile Acid Synthesis and Transport

Symbol	Description	$-/-$ ND vs $+/-$ ND	$+/-$ HCD vs $+/-$ ND	$-/-$ HCD vs $+/-$ ND	Cellular localization
<b>Bile synthesis</b>					
Acox2	Acyl-CoA oxidase 2, branched chain	1.08	0.83	2.54 <sup>a</sup>	Mitochondrion, peroxisome
Amacr	$\alpha$ -Methylacyl-CoA racemase	1.07	0.99	2.34 <sup>a</sup>	Mitochondrion, peroxisome
Cyp8b1	Cytochrome P450, family 8, subfamily b, polypeptide 1	0.97	0.99	2.09 <sup>a</sup>	ER
Acot8	Acyl-CoA thioesterase 8	1.05	0.91	0.49 <sup>a</sup>	Mitochondrion, peroxisome
<b>Bile transport and secretion</b>					
Abcc2	ATP-binding cassette, subfamily C, member 2	0.97	1.34	3.51 <sup>a</sup>	Membrane
Slc10a1	Solute carrier family 10 (sodium/bile acid cotransporter), member 1	1.69 <sup>b</sup>	1.28	3.49 <sup>a</sup>	Cell membrane
Slc22a7	Solute carrier family 22 (organic anion transporter), member 7	1.17	0.98	3.85 <sup>a</sup>	Cell membrane
Slc22a1	Solute carrier family 22 (organic cation transporter), member 1	1.16	0.95	2.25 <sup>a</sup>	Cell membrane
Slc27a5	Solute carrier family 27 (fatty acid transporter), member 5	1.36	0.98	4.37 <sup>a</sup>	ER
Slco1a1	Solute carrier organic anion transporter family, member 1a1	0.94	0.86	6.44 <sup>a</sup>	Cell membrane
Slco1a4	Solute carrier organic anion transporter family, member 1a4	1.30	2.45 <sup>a</sup>	10.96 <sup>a</sup>	Cell membrane
Slco1b2	Solute carrier organic anion transporter family, member 1B2	1.35	0.88	2.41 <sup>a</sup>	Cell membrane
Stard10	Steroidogenic acute regulatory protein-related lipid transfer domain containing 10	1.38	1.14	2.58 <sup>a</sup>	Cell membrane
Sult2a1	Sulfotransferase family 2A, dehydroepiandrosterone-preferring, member 1	1.53 <sup>b</sup>	1.06	6.69 <sup>a</sup>	Cytoplasm
Sult2a1	Sulfotransferase family 2A, dehydroepiandrosterone-preferring, member 1	2.09 <sup>a</sup>	1.00	4.40 <sup>a</sup>	Cytoplasm
Abcb1a	ATP-binding cassette, subfamily B, member 1A	0.55 <sup>b</sup>	1.34	0.34 <sup>a</sup>	Cell membrane
Abcc3	ATP-binding cassette, subfamily C, member 3	0.65 <sup>b</sup>	0.57 <sup>b</sup>	0.08 <sup>a</sup>	Cell membrane
Ephx1	Epoxide hydrolase 1, microsomal (xenobiotic)	0.77	1.23	0.35 <sup>a</sup>	ER
Ldlr	Low-density lipoprotein receptor	0.99	0.65 <sup>b</sup>	0.49 <sup>a</sup>	Cell membrane, Golgi
Abcb11	ATP-binding cassette, subfamily B, member 11	1.00	1.14	1.06	Cell membrane

NOTE. Data are presented as mean ratios from 3 age-matched animals (age, 80–82 days). ER, endoplasmic reticulum.

<sup>a</sup>Fold-changes greater than 2 compared with  $+/-$  ND control.

<sup>b</sup>Fold-changes between 1.5 and 2.0 compared with  $+/-$  ND control.

fatty acid degradation were enriched in livers of HCD-fed  $Atp7b^{+/-}$  rats, but especially in HCD-fed  $Atp7b^{-/-}$  rat livers (Table 4). Interestingly, we also observed higher abundancies of lipid biosynthesis enzymes, partly in HCD-fed  $Atp7b^{+/-}$  control rats, but very prominently in HCD-fed  $Atp7b^{-/-}$  rats (Table 5). Although these increased enzyme abundancies do not necessarily mean an enhanced flux via these pathways, the highly increased supply of fatty acids via the HCD vs ND<sup>14</sup> indicates a 2-fold adaptation in hepatocytes: first, their increased degradation in mitochondria

via  $\beta$ -oxidation, and, second, their esterification to triglycerides that are preferentially stored in cytosol. Future measurements have to validate such enhanced metabolic fluxes and/or specific metabolites from these pathways. Furthermore, besides the mere levels of enzyme abundancies, metabolic enzyme activities may be modulated further via post-translational modifications such as acetylation and succinylation,<sup>42</sup> which were not assessed in this study. Indeed, increased acetyl-CoA levels from augmented  $\beta$ -oxidation may result in increased acetylation<sup>43</sup> of

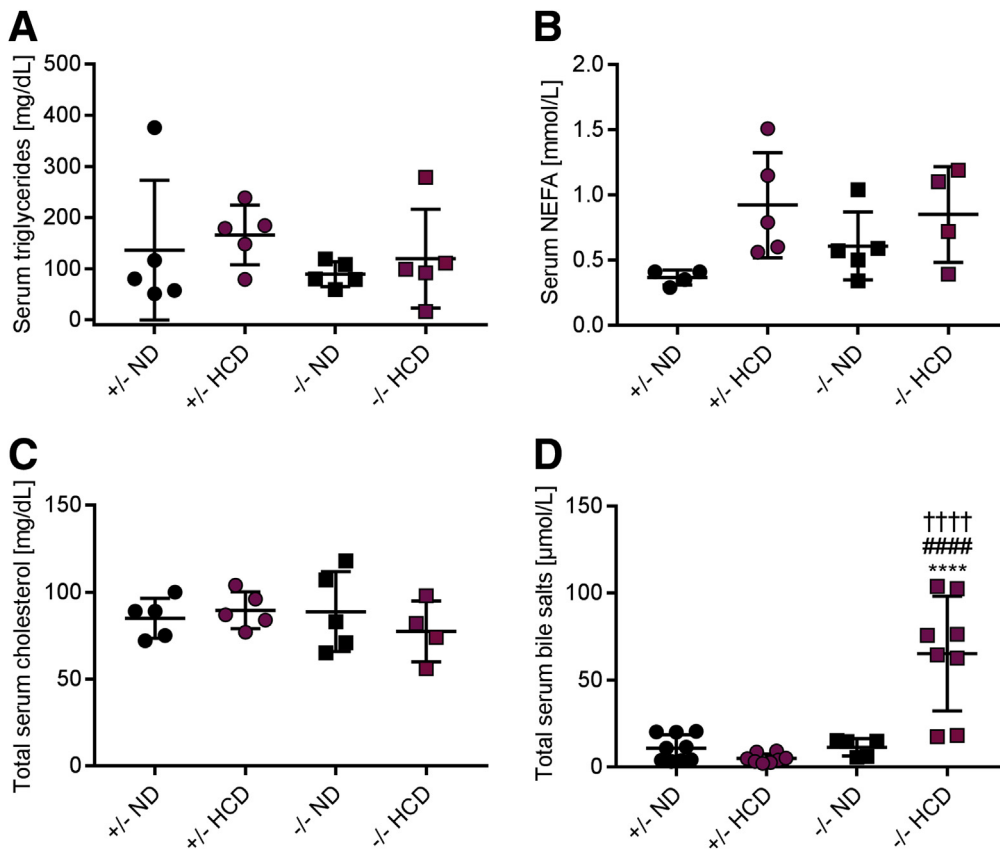


**Figure 6.** An HCD increases total serum bile salts in *Atp7b*<sup>-/-</sup> rats. (A) Serum triglycerides, (B) serum nonesterified fatty acids (NEFAs), and (C) total serum cholesterol do not differ between ND and HCD groups (N = 4–5). (D) Total serum bile salts increase in HCD-fed *Atp7b*<sup>-/-</sup> rats (N = 3–5). One-way analysis of variance with the Tukey multiple comparisons test. \*Significant to *Atp7b*<sup>+/-</sup> ND. #Significant to *Atp7b*<sup>+/-</sup> HCD. †Significant to *Atp7b*<sup>-/-</sup> ND. \*,#†P < .05; \*\*,##,††P < .01; \*\*\*,###,†††P < .001; \*\*\*\*,####,††††P < .0001.

mitochondrial enzymes involved in the tricarboxylic acid cycle, fatty acid oxidation, amino acid and carbohydrate metabolism, ketone body synthesis, and the urea cycle.<sup>42,44</sup> Moreover, an increasing acetyl-CoA amount would influence not only these pathways, but also possibly would cause increased cholesterol levels because acetyl-CoA is the precursor in hepatic cholesterol biosynthesis.<sup>32</sup> Such hepatic cholesterol accumulation has been reported in NAFLD patients and rodents<sup>45</sup> and correlated with histologic severity of the disease and thus seems to be associated with HCD malnutrition. In fact, increased enzyme abundancies for nearly the whole cholesterol biosynthesis pathway were found in HCD-fed *Atp7b*<sup>-/-</sup> rat livers (Table 6). Unexpectedly, however, we did not observe specifically increased cholesterol levels in these animals (Figure 6C). This may have been prevented by an increased routing of cholesterol into bile salts because we determined 2- to 11-fold increases in abundancies of enzymes involved in bile salt synthesis and bile excretion in HCD-fed *Atp7b*<sup>-/-</sup> rat livers (Table 7). In agreement, we found increased serum bile salts only in serum of HCD-fed *Atp7b*<sup>-/-</sup> rats (Figure 6D), which were reduced significantly upon MB treatment (Figure 8C). Clearly, such increased bile salt synthesis may be a further detrimental impact in HCD-fed *Atp7b*<sup>-/-</sup> rat livers because accumulating bile salts are hepatotoxic (especially to hepatic mitochondria).<sup>46,47</sup>

In conclusion, the combination of accumulating copper with an HCD is highly detrimental to hepatic mitochondria.

A toxic triad of ATP depletion, massively increased ROS, and bile salts seals the fate of affected hepatocytes. This indicates that a high- vs normal-calorie nutrition may have a tremendous impact on WD progression and severity and may contribute to the striking phenotype–genotype discrepancies encountered in WD patients, in agreement with a recent review article that indicated the importance of lifestyle modifications in WD.<sup>18</sup> We therefore suggest monitoring such aspects of nutrition in much more detail in the future, to establish whether dietary counseling of WD patients may be of therapeutic benefit.

## Materials and Methods

### Animal Studies

Animals were maintained under the Guidelines for the Care and Use of Laboratory Animals of the Helmholtz Center Munich. Animal experiments were approved by the government authorities of the Regierung von Oberbayern, Munich, Germany.

Control *Atp7b*<sup>+/-</sup> and WD *Atp7b*<sup>-/-</sup> rats of both sexes (Table 2; strain name, LPP crossbreed between Long Evans cinnamon rats and Piebald Virol Glaxo rats; bred in-house, provided by Borjigin) were used because we currently have no indication for a sex-dependent altered WD phenotype in these animals.<sup>3</sup> Animals were fed ad libitum either on an ND (1314; Altromin Spezialfutter GmbH, Seelenkamp, Germany; copper content, 13.9 mg/kg; metabolic energy,

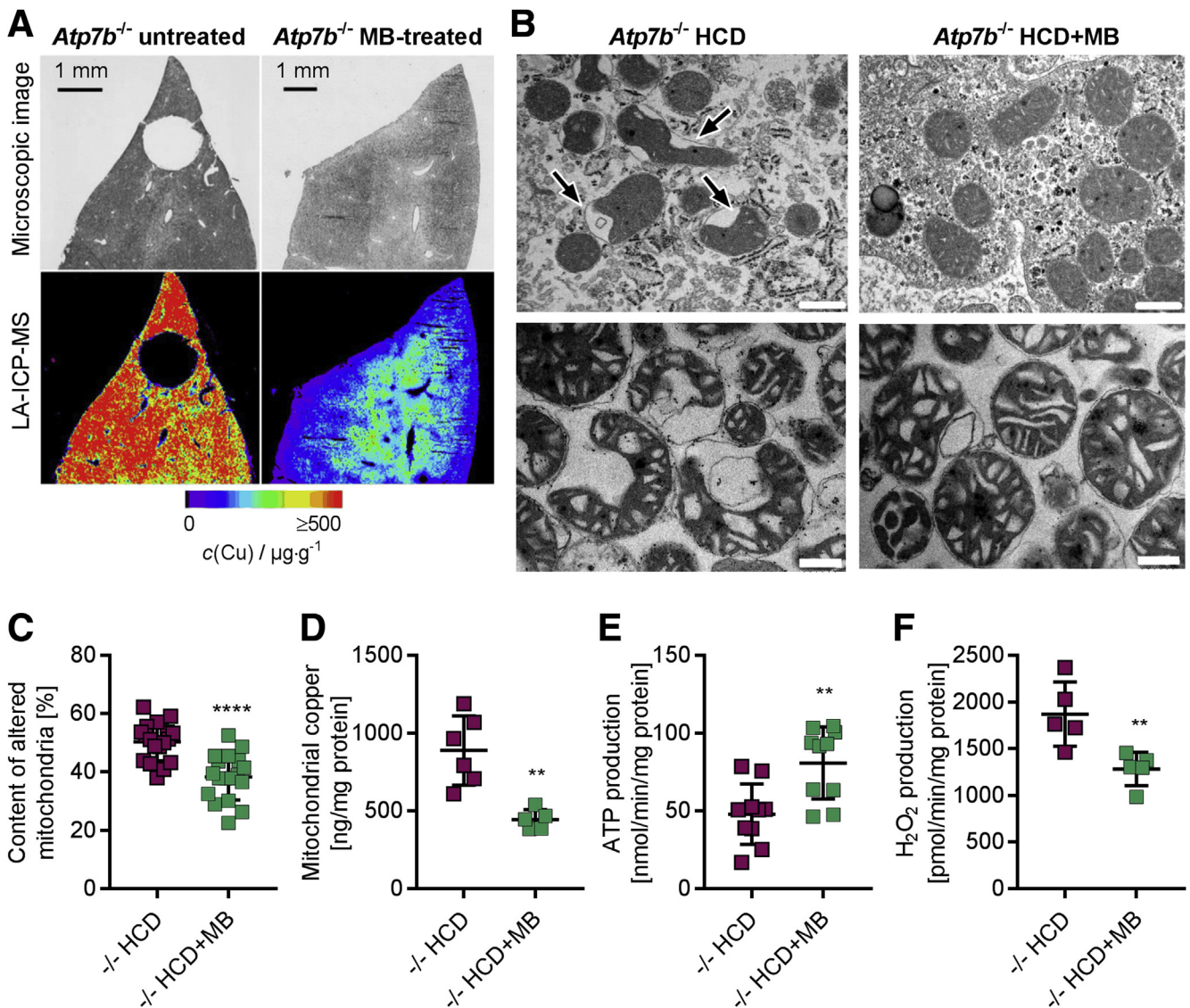


**Figure 7. MB rescues HCD-induced mitochondrial dysfunction in *Atp7b*<sup>-/-</sup> rats.** (A) Laser ablation ICP-MS distribution maps (lower panels) show lower copper concentrations in liver samples from ND-fed, MB-treated *Atp7b*<sup>-/-</sup> rats compared with untreated ND-fed *Atp7b*<sup>-/-</sup> controls (copper concentration range, 0–500  $\mu\text{g}/\text{g}$ ; laser spot size, 25  $\mu\text{m}$ ; scan speed, 50  $\mu\text{m}/\text{s}$ ). (B) Electron micrographs of mitochondria either in situ (upper panel, scale bar: 500 nm) or isolated (lower panel, scale bar: 500 nm) show mitochondrial structure normalization upon MB treatment (right panels) vs untreated (left panels). (C) Quantification of isolated mitochondria with altered structure (N = 3, 700–750 mitochondria in each animal group). (D–F) Methanobactin treatment (D) decreases mitochondrial copper load (N = 5–6), (E) increases mitochondrial ATP production (N = 5), and (F) decreases mitochondrial H<sub>2</sub>O<sub>2</sub> emergence (substrates, glutamate/malate; N = 5). Unpaired *t* test, significant if \*\**P* < .01; \*\*\*\**P* < .0001.

3301 kcal/kg; 14% kcal from fat) and tap water (copper content, <0.2 mg/L) or on an HCD (Altromin Spezialfutter GmbH; copper content, 9.3 mg/kg; metabolic energy, 4523 kcal/kg; 45% kcal from fat) and fructose syrup (metabolic energy, 722 kcal/L) in drinking water supplemented with 3.1 mg/L copper.<sup>14,24</sup> Rats were fed an HCD starting at an age of 46–50 days until an age of 79–82 days. To additionally test for a difference in the age of onset and rate of liver damage progression on the 2 diets (HCD vs ND), a subset of animals was analyzed in parallel at an age of 67,

73, and 75 days (Table 2). Daily consumption values for rats were estimated from the literature to be approximately 20 g chow and 30 mL water, respectively.<sup>48</sup> In subsequent control measurements in *Atp7b*<sup>+/-</sup> rats, we determined an average uptake of 16.1 ± 1.7 g ND food and 31 ± 3 mL water per day (ie, approximately 230  $\mu\text{g}$  copper/day), and 12.5 ± 1.7 g HCD food and 50 ± 15 mL fructose syrup (ie, approximately 272  $\mu\text{g}$  copper/day). Thus, the HCD/sugar-water diet supplied slightly more copper (approximately 18%) compared with the ND/tap water diet, but

**Table 8.** MB Treatment (Intraperitoneally, Once Daily for 5 Days) Reduces Liver Damage and Copper Overload in Serum, Kidney, and Livers of Female HCD-Fed *Atp7b*<sup>-/-</sup> Rats

Animal ID	Rat 38	Rat 39	Rat 40	Rat 41	Rat 42	-/- HCD + MB, mean	-/- HCD, mean
Sex	Female	Female	Female	Female	Female		
Age, day	79	79	80	80	80	80 <sup>a</sup>	74 <sup>a</sup>
AST, U/L							
Before	227	330	419	368	545	378	300
After	172	123	196	136	136	191	nd
Bilirubin, mg/dL							
Before	<0.5	<0.5	<0.5	<0.5	1.2	<0.5 <sup>a</sup>	<0.5 <sup>a</sup>
After	<0.5	<0.5	<0.5	<0.5	<0.5	<0.5 <sup>a</sup>	nd
Body weight, g							
Before	121	141	128	122	102	123	146
After	126	149	134	132	113	131	nd
Spleen weight, g	0.23	0.15	0.25	0.23	0.28	0.23	0.28
Visceral fat, g	1.93	2.39	2.66	1.99	2.04	2.20	2.53
Serum Cu, ng/mL	n.d.	455	296	224	525	375	640
Kidney Cu, μg/g wet weight	36	40	62	44	100	56	99
Liver homogenate Cu, μg/g wet weight	318	237	247	296	284	276	392
Mitochondrial Cu, ng/mg protein	538	384	386	445	467	444	893 <sup>b</sup>
Mitochondrial Cu depletion, % <sup>b</sup>	39.8	57.0	56.7	50.1	47.7	50	0
NAS	4	5	4	5	5	5a	6 <sup>a</sup>
HAI	8	10	8	12	12	10 <sup>a</sup>	11 <sup>a</sup>

NOTE. Data on AST, bilirubin, and body weight are present before and after 5 days of MB treatment. NAFLD activity score was as follows: ≤2, no nonalcoholic steatohepatitis; 3–4, borderline nonalcoholic steatohepatitis; ≥5 definite nonalcoholic steatohepatitis.

Cu, copper; nd, not determined.

<sup>a</sup>Values are shown as medians.

<sup>b</sup>Mitochondrial copper depletion relative to the mean mitochondrial copper value of female untreated *Atp7b*<sup>-/-</sup> rats.

nevertheless resulted in almost equal liver homogenate copper contents in both *Atp7b*<sup>+/-</sup> rats and *Atp7b*<sup>-/-</sup> rats (Figure 3C). MB treatment of HCD-fed *Atp7b*<sup>-/-</sup> rats was performed once daily for 5 consecutive days starting at an age of 74–75 days, as recently described (150 mg/kg body weight intraperitoneally).<sup>5</sup>

### Chemicals

Chemicals were mostly obtained from Sigma–Aldrich (Taufkirchen, Germany). Nitric acid, K<sub>2</sub>HPO<sub>4</sub>, KCl, malate, iodacetamide, multi-element standard IV, copper (II) sulfate pentahydrate, ethanol, and xylene were purchased from Merck (Darmstadt, Germany). Acetyl-CoA, reduced nicotinamide adenine dinucleotide (NADH), phosphoenolpyruvate, pyruvate kinase and lactate dehydrogenase were obtained from Roche Diagnostics (Mannheim, Germany). Bovine serum albumin (BSA) and 4-(2-hydroxyethyl)-1-piperazineethanesulfonic acid (HEPES) were purchased from Carl-Roth (Karlsruhe, Germany). Tris-(hydroxymethyl) aminomethane (TRIS) was obtained from VWR International GmbH (Ismaning, Germany). Gelatin was purchased from Grüssing (Filsum, Germany). Rhodium Inductively Coupled Plasma (ICP) standard solution was purchased from SCP Science (Baie D'Urfé, Canada). Osmium tetroxide and uranyl-less contrasting agent were obtained from

Science Services GmbH (Munich, Germany). Propylene oxide and epoxy resin were purchased from SERVA Electrophoresis GmbH (Heidelberg, Germany). Lead citrate was purchased from Leica Biosystems (Wetzlar, Germany).

### Liver Examination

Serum AST and bilirubin levels were measured with the Reflotron system (Roche Diagnostics, Penzberg, Germany) and liver damage in animals was considered clinically apparent if the serum AST level was greater than 200 U/L and/or the bilirubin level was greater than 0.5 mg/dL.<sup>5</sup> Serum cholesterol nonesterified fatty acids and serum triglycerides were analyzed with ResponS910 (Diasys Greiner GmbH, Flacht, Germany) according to the manufacturer's guidelines. Serum ceruloplasmin activity was measured as described elsewhere.<sup>49,50</sup> Total serum bile salt concentrations were quantified in serum samples using the Diazyme total bile salt kit (Diazyme Laboratories, Poway, CA) according to the manufacturer's instructions. Histologic evaluation was performed on formalin-fixed, paraffin-embedded H&E-stained liver samples. Morphologic features were summarized as an activity score as recommended for the diagnosis of steatohepatitis in NAFLD (NAS)<sup>25</sup> as well as for hepatitis (HAI score).<sup>51</sup> For quantification of liver triglycerides, 100 mg/mL liver tissue was sonicated within 5% NP40 solution,



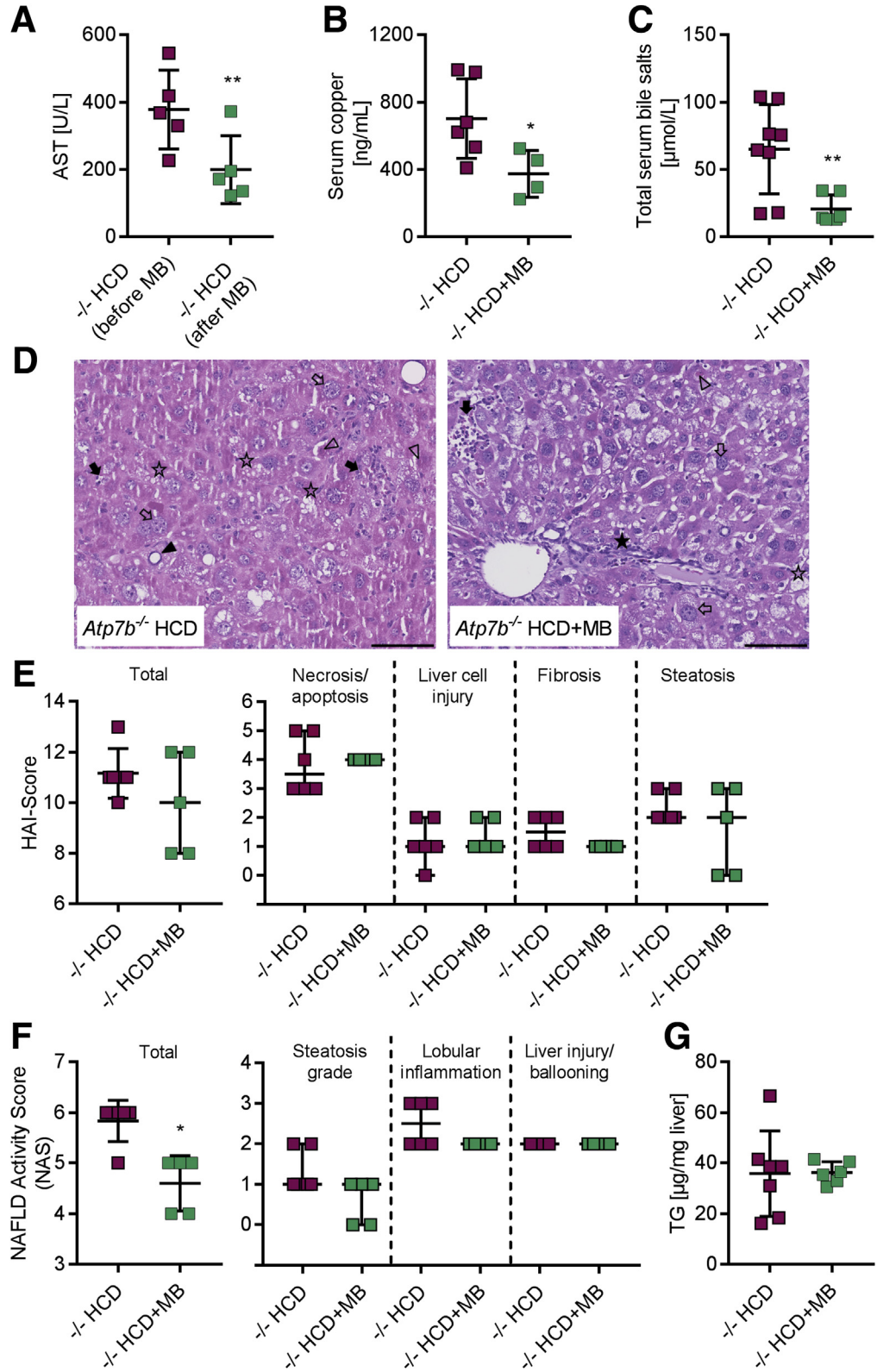


**Figure 8.** MB rescues overt/acute liver damage in HCD-fed *Atp7b*<sup>-/-</sup> rats. (A–C) Short-term MB treatment (A) significantly reduces the liver damage marker AST (comparison of HCD-fed *Atp7b*<sup>-/-</sup> rats before and after MB treatment), and (B and C) significantly decreases serum copper and bile salts (comparison of HCD-fed *Atp7b*<sup>-/-</sup> rats with vs without MB treatment). (D) Liver sections (scale bar: 100 μm) from MB-treated (right panel) vs untreated HCD-fed *Atp7b*<sup>-/-</sup> rats (left panel) showed no significant reduction of lobular inflammation (black arrow), apoptosis (open arrowhead), necrosis (black arrowhead), fibrosis (black asterisk), or steatosis (open asterisk), as also evidenced by only slightly lower (E) HAI score and (F) NAS. (G) Liver triglyceride content was unchanged after MB treatment. (A–C, and G) Unpaired *t* test (N = 3–6), significant if \**P* < .05, means ± SD; (E and F) nonparametric Mann–Whitney test (N = 5–6), significant if \**P* < .05, medians ± range.

heated for 5 minutes at 96°C, and cooled on ice. Homogenates were cleared for 2 minutes at 20,000×*g*, and supernatants (diluted in 5% NP40 solution 1:1–1:10 as required) were analyzed with Respons910 (Diasys Greiner GmbH).<sup>13</sup>

**Metal Content Determination**

Copper in serum, liver homogenate, cytosol, and mitochondria, as well as kidney homogenate, were analyzed by ICP Optical Emission Spectrometry (Ciros Vision, SPECTRO

Analytical Instruments GmbH, Kleve, Germany) after wet ashing of samples with 65% nitric acid.<sup>4</sup>

### Preparation of Rat Liver Cytosol and Mitochondria

Freshly removed liver tissue was homogenized with a Teflon-glass homogenizer (B. Braun Biotech, Melsungen, Germany) in isolation buffer (pH 7.2) containing 300 mmol/L sucrose, 5 mmol/L 2-[(2-hydroxy-1,1-bis(hydroxymethyl)ethyl)amino]ethanesulfonic acid (TES), 0.2 mmol/L ethylene glycol-bis( $\beta$ -aminoethyl ether)-*N,N,N',N'*-tetraacetic acid (EGTA), and 0.1% BSA. Approximately 1 mL of the homogenate was centrifuged at 100,000 $\times g$  (1 h, 4°C), and the supernatant (liver cytosol) was collected and stored at -80°C.

For mitochondrial isolation, the remaining homogenate was cleared from debris and nuclei by an 800 $\times g$  (10 min at 4°C) centrifugation step, and a crude mitochondrial fraction was pelleted at 18,900 $\times g$  (20 min at 4°C). To purify mitochondria, the pellet was suspended in isolation buffer, loaded on a Nycodenz gradient (Axis-Shield PoC, Oslo, Norway; gradient composition was as follows: 1 mL of 40%, 1 mL of 33%, 3 mL of 28%, 2 mL of 27%, 2 mL of 24% Nycodenz solution; diluted in 10 mmol/L TRIS, pH 7.4), and centrifuged at 74,100 $\times g$  (1 h, 4°C). The mitochondrial fraction (layer at the 28% gradient phase) was collected and suspended in isolation buffer without BSA and washed 2 times at 18,900 $\times g$  (10 min at 4°C).<sup>52-54</sup>

### Mitochondrial ATP Production

ATP production was determined using the ATP Bioluminescence Assay Kit (Roche Diagnostics, Mannheim, Germany) according to the manufacturer's guideline. In detail, 10  $\mu g$  mitochondria were incubated with 160  $\mu mol/L$  adenosine diphosphate (ADP) and 5 mmol/L succinate for 30 minutes at room temperature in a buffer containing 0.2 mol/L sucrose, 10 mmol/L 3-(*N*-morpholino)propanesulfonic acid-TRIS, 1 mmol/L inorganic phosphate, 10  $\mu mol/L$  EGTA and 2  $\mu mol/L$  rotenone. As background control, potassium cyanide (2 mmol/L, respiratory chain complex IV inhibitor) was added. Mitochondrial ATP production was calculated in pmol/min/mg protein based on background-corrected luminescence signals and ATP standard curves (Roche Diagnostics, Mannheim, Germany).

### Mitochondrial Respiration

Mitochondrial respiration was measured with an Oxygraph-2k instrument and processed via DatLab 6.2 software (Oroboros Instruments, Innsbruck, Austria). Per each chamber, 100  $\mu g$  mitochondria was supplied in a buffer containing 0.25 mol/L sucrose, 1 mmol/L EGTA, 30 mmol/L  $K_2HPO_4$ , 15 mmol/L KCl, 5 mmol/L  $MgCl_2$ , 25 mmol/L succinate, 1  $\mu mol/L$  rotenone, and 0.5 mmol/L ADP, and oxygen consumption rates were measured as succinate-linked phosphorylation. To determine leak respiration, 2.5 mmol/L oligomycin was added (final, 2.5  $\mu mol/L$ ) to block ATP synthase. Subsequently, the protonophore carbonyl

cyanide-4-(trifluoromethoxy)phenylhydrazone was titrated (2  $\mu L$  steps from a 20  $\mu mol/L$  stock solution) to induce maximum oxygen consumption (electron transfer system capacity). The respiratory control ratio was calculated by dividing the succinate-linked phosphorylation oxygen consumption by the oxygen consumption upon oligomycin addition.

### Mitochondrial $H_2O_2$ Production

Mitochondrial  $H_2O_2$  production was analyzed after resorufin fluorescence<sup>55</sup> (converted from Amplex Red; Molecular Probes, Invitrogen, Karlsruhe, Germany) at  $\lambda_{Ex}$  540/20 nm and  $\lambda_{Em}$  620/40 nm. The assay was performed with 75  $\mu g$  mitochondria in 150  $\mu L$  buffer (pH 7.4) containing 125 mmol/L KCl, 10 mmol/L 4-(2-hydroxyethyl)-1-piperazineethanesulfonic acid, 5 mmol/L  $MgCl_2$ , 2 mmol/L  $K_2HPO_4$ , 5  $\mu mol/L$   $MnCl_2$ , and as substrates either 10 mmol/L succinate/2  $\mu mol/L$  rotenone and 3.2 mmol/L ADP, or 5 mmol/L glutamate/5 mmol/L malate. To start the reaction, 50  $\mu L$  of a solution containing 320  $\mu mol/L$  Amplex Red, 2 U/mL horseradish peroxidase, and 60 U/mL superoxide dismutase was added. Resorufin fluorescence was followed up in a plate reader (Synergy 2; BioTek Instruments, Inc, Bad Friedrichshall, Germany) and the Resorufin slope was converted into the rate of  $H_2O_2$  production in pmol/min/mg with a  $H_2O_2$  standard curve.<sup>55</sup>

### $F_1F_0$ -Activity and Citrate Synthase Activity

$F_1F_0$  activity was assessed as described before.<sup>13,56</sup> In detail, 20  $\mu g$  mitochondria were incubated in buffer containing either 50 mmol/L TRIS (pH 8.0) or an additional 3  $\mu mol/L$  oligomycin ( $F_1F_0$  inhibitor, negative control) for 5 minutes at 37°C in a plate reader (Synergy 2). To start the reaction, a final mixture of 0.5 mmol/L ATP, 3  $\mu mol/L$  carbonyl cyanide 3-chlorophenylhydrazone, 1 mg/mL BSA, 1  $\mu mol/L$  antimycin A, 10 mmol/L KCl, 4 mmol/L  $MgCl_2$ , 0.2 mmol/L NADH, 2 mmol/L phosphoenolpyruvate, 4 U lactate dehydrogenase, and pyruvate kinase were added. The  $F_1F_0$  activity was determined in the reverse direction after ATP hydrolysis and NADH oxidation in parallel to the conversion of pyruvate to lactate. The decrease in NADH absorbance at 340 nm was proportional to the ATPase activity and was calculated in nmol/min/mg protein. The  $F_1F_0$  activity was normalized to the activity of the housekeeping enzyme citrate synthase (CS). The activity of mitochondrial CS was determined according to earlier reports.<sup>57,58</sup> In brief, 280  $\mu L$  of a solution containing 2.5% (wt/vol) Triton X-100, 100  $\mu mol/L$  5,5'-dithiobis-(2-nitrobenzoic acid), 75  $\mu g$  acetyl-CoA, and 500  $\mu mol/L$  oxaloacetate was incubated at 37°C. The reaction was started by adding 20  $\mu g$  mitochondria and followed at 412 nm for 5 minutes. CS activities were calculated from the linear slopes of the initial rates.<sup>56</sup>

### Electron Microscopy

Animal livers and isolated mitochondria were fixed with 2.5% glutaraldehyde (Science Services GmbH), postfixed with 1% osmium tetroxide, dehydrated with ethanol and propylene oxide, and were embedded in epoxy resin. Sixty-

nanometer sections were cut using the Leica EM UC7 microtome (Leica Biosystems) or the Reichert-Jung Ultracut E microtome (now Leica Biosystems). Ultrathin sections were negative-stained with uranyl acetate (Uranyless) and lead citrate. Images were acquired using either a FEI Tecnai-12 electron microscope equipped with a VELETTA CCD digital camera (FEI, Eindhoven, The Netherlands) or using a Jeol 1200 EXII electron microscope (Akishima, Tokyo, Japan) equipped with a KeenViewII digital camera (Olympus, Hamburg, Germany) and processed with the iTEM software package (anlySISFive; Olympus).

For structural analyses, mitochondria were grouped in normally structured mitochondria of the “condensed type”<sup>59</sup> or in altered mitochondria with marked membrane detachments, matrix condensations, and ballooned cristae. A total of 350–750 mitochondria were included per group of animals.

### Proteome Analysis

**Mass spectrometry (MS) sample preparation.** Liver homogenates were lysed in urea buffer (9 mol/L urea, 6 mol/L thiourea, 65 mmol/L dithiothreitol). A total of 10  $\mu$ g protein per replicate was proteolytically cleaved by applying a modified filter-aided sample preparation procedure,<sup>14</sup> including a quenching step using 1 mol/L dithiothreitol to bind unreacted iodacetamide. After elution of peptides, samples were acidified with 0.5% trifluoroacetic acid and analyzed on the OrbitrapXL (Thermo Fisher Scientific, Dreieich, Germany) as described.<sup>14,60</sup>

**Mass spectrometry.** Liquid chromatography tandem-mass spectrometry analysis was performed on a LTQ-Orbitrap XL operated on a nano-high-performance liquid chromatography (UltiMate 3000 RSLCnano System; Thermo Fisher Scientific) as described elsewhere,<sup>14,61</sup> with the modification of using a nonlinear 300-minute liquid chromatography gradient.

**Protein identification and label-free relative quantification.** Acquired spectra were analyzed using Progenesis QI for proteomics (v2.0; Nonlinear Dynamics, Newcastle upon Tyne, UK), as described previously,<sup>14</sup> with the following adaptations: spectra were searched using the search engine Mascot (version 2.5.1; Matrix Science, London, UK) against the Ensembl rat database (release 80; 28,609 sequences). The Mascot-integrated decoy database search using the Percolator algorithm was set to a peptide false discovery rate of less than 1.5%. Peptide assignments were imported into Progenesis QI. Normalized abundances of peptides were summed up and allocated to the respective protein.

### Laser Ablation ICP-Mass Spectrometry

For laser ablation ICP-MS analysis, tissue sections of rat liver samples embedded in paraffin were prepared with a thickness of 5  $\mu$ m using a microtome HM 355S (Thermo Scientific, Bremen, Germany). To quantify the copper concentration in the tissue samples, matrix-matched standards based on 10% gelatin in aqueous solutions of copper (II) sulfate pentahydrate were prepared as described before.<sup>62</sup> The concentration range for copper was between 10 and

1000  $\mu$ g/g. To validate the standard concentrations, bulk analysis after digestion with nitric acid was used as described before.<sup>62</sup> A laser ablation system (LSX-213 G2+; Teledyne CETAC Technologies, Omaha, NE) was used. ICP-MS detection was performed with a quadrupole-based iCAP TQ (Thermo Fisher Scientific). The laser ablation and ICP-MS were connected with Tygon tubing Saint-Gobain (Courbevoie, France). The following ICP-MS parameters were applied for all measurements: forward power, 1550 W; cool gas flow, 14 L/min; and auxiliary gas flow, 0.8 L/min. In-house-developed software was used to convert the laser ablation ICP-MS data into 2-dimensional images. The copper concentration was calculated using a linear calibration function derived from the average signal intensities for each standard using Microsoft Excel 2016 (Microsoft Corp, Redmond, WA).

### Miscellaneous

MB was isolated from the spent media of *Methylosinus trichosporium* OB3b as previously described.<sup>63</sup> Protein quantification was performed by the Bradford<sup>64</sup> or Biuret assay (T1949; Sigma-Aldrich).

### Statistics

Throughout this study, N refers to the number of analyzed animals. Data are presented as means  $\pm$  SD. Statistical significance was analyzed using 1-way analysis of variance with the Tukey multiple comparisons test, or the nonparametric Kruskal–Wallis test when comparing 3 or more sample sets (GraphPad Prism 7, GraphPad Software, Inc, San Diego, CA). For 2 group comparisons, the unpaired 2-tailed Student *t* test was used for parametric data and the Mann–Whitney test was used for nonparametric data, respectively (GraphPad Prism 7).

All authors had access to the study data and reviewed and approved the final manuscript.

### References

1. Ferenci P. Phenotype-genotype correlations in patients with Wilson’s disease. *Ann N Y Acad Sci* 2014;1315:1–5.
2. Ferenci PCA, Stremmel W, Houwen R, Rosenberg W, Schilsky M, Jansen P, Moradpour D. EASL clinical practice guidelines: Wilson’s disease. *J Hepatol* 2012; 56:671–685.
3. Ahmed S, Deng J, Borjigin J. A new strain of rat for functional analysis of PINA. *Brain Res Mol Brain Res* 2005;137:63–69.
4. Zischka H, Lichtmanegger J, Schmitt S, Jagemann N, Schulz S, Wartini D, Jennen L, Rust C, Larochette N, Galluzzi L, Chajes V, Bandow N, Gilles VS, DiSpirito AA, Esposito I, Goettlicher M, Summer KH, Kroemer G. Liver mitochondrial membrane crosslinking and destruction in a rat model of Wilson disease. *J Clin Invest* 2011; 121:1508–1518.
5. Lichtmanegger J, Leitzinger C, Wimmer R, Schmitt S, Schulz S, Kabiri Y, Eberhagen C, Rieder T, Janik D, Neff F, Straub BK, Schirmacher P, DiSpirito AA, Bandow N,



- Baral BS, Flatley A, Kremmer E, Denk G, Reiter FP, Hohenester S, Eckardt-Schupp F, Dencher NA, Adamski J, Sauer V, Niemiets C, Schmidt HH, Merle U, Gotthardt DN, Kroemer G, Weiss KH, Zischka H. Methanobactin reverses acute liver failure in a rat model of Wilson disease. *J Clin Invest* 2016;126:2721–2735.
6. Choi DW, Zea CJ, Do YS, Semrau JD, Antholine WE, Hargrove MS, Pohl NL, Boyd ES, Geesey GG, Hartsel SC, Shafe PH, McEllistrem MT, Kisting CJ, Campbell D, Rao V, de la Mora AM, Dispirito AA. Spectral, kinetic, and thermodynamic properties of Cu(I) and Cu(II) binding by methanobactin from *Methylosinus trichosporium* OB3b. *Biochemistry* 2006;45:1442–1453.
  7. El Ghazouani A, Basle A, Firbank SJ, Knapp CW, Gray J, Graham DW, Dennison C. Copper-binding properties and structures of methanobactins from *Methylosinus trichosporium* OB3b. *Inorg Chem* 2011;50:1378–1391.
  8. Sternlieb I. Mitochondrial and fatty changes in hepatocytes of patients with Wilson's disease. *Gastroenterology* 1968;55:354–367.
  9. Stattermayer AF, Traussnigg S, Dienes HP, Aigner E, Stauber R, Lackner K, Hofer H, Stift J, Wrba F, Stadlmayr A, Datz C, Strasser M, Maieron A, Trauner M, Ferenci P. Hepatic steatosis in Wilson disease—role of copper and PNPLA3 mutations. *J Hepatol* 2015;63:156–163.
  10. Vernon G, Baranova A, Younossi ZM. Systematic review: the epidemiology and natural history of non-alcoholic fatty liver disease and non-alcoholic steatohepatitis in adults. *Aliment Pharmacol Ther* 2011;34:274–285.
  11. Cortez-Pinto H, Chatham J, Chacko VP, Arnold C, Rashid A, Diehl AM. Alterations in liver ATP homeostasis in human nonalcoholic steatohepatitis: a pilot study. *JAMA* 1999;282:1659–1664.
  12. Caldwell SH, Swerdlow RH, Khan EM, Iezzoni JC, Hespeneheide EE, Parks JK, Parker WD Jr. Mitochondrial abnormalities in non-alcoholic steatohepatitis. *J Hepatol* 1999;31:430–434.
  13. Einer C, Hohenester S, Wimmer R, Wottke L, Artmann R, Schulz S, Gosmann C, Simmons A, Leitzinger C, Eberhagen C, Borchard S, Schmitt S, Hauck SM, von Toerne C, Jastroch M, Walheim E, Rust C, Gerbes AL, Popper B, Mayr D, Schnurr M, Vollmar AM, Denk G, Zischka H. Mitochondrial adaptation in steatotic mice. *Mitochondrion* 2018;40:1–12.
  14. Einer C, Hohenester S, Wimmer R, Wottke L, Artmann R, Schulz S, Gosmann C, Simmons A, Leitzinger C, Eberhagen C, Borchard S, Schmitt S, Hauck SM, von Toerne C, Jastroch M, Walheim E, Rust C, Gerbes AL, Popper B, Mayr D, Schnurr M, Vollmar AM, Denk G, Zischka H. Data on chow, liver tissue and mitochondrial fatty acid compositions as well as mitochondrial proteome changes after feeding mice a western diet for 6–24 weeks. *Data Brief* 2017;15:163–169.
  15. Pfeiffer RF. Wilson's disease. *Handb Clin Neurol* 2011;100:681–709.
  16. Brewer GJ, Yuzbasiyan-Gurkan V, Dick R, Wang Y, Johnson V. Does a vegetarian diet control Wilson's disease? *J Am Coll Nutr* 1993;12:527–530.
  17. Kegley KM, Sellers MA, Ferber MJ, Johnson MW, Joelson DW, Shrestha R. Fulminant Wilson's disease requiring liver transplantation in one monozygotic twin despite identical genetic mutation. *Am J Transplant* 2010;10:1325–1329.
  18. Kieffer DA, Medici V. Wilson disease: at the crossroads between genetics and epigenetics—a review of the evidence. *Liver Res* 2017;1:121–130.
  19. Yamazaki K, Ohyama H, Kurata K, Wakabayashi T. Effects of dietary vitamin E on clinical course and plasma glutamic oxaloacetic transaminase and glutamic pyruvic transaminase activities in hereditary hepatitis of LEC rats. *Lab Anim Sci* 1993;43:61–67.
  20. Kitamura Y, Nishikawa A, Nakamura H, Furukawa F, Imazawa T, Umemura T, Uchida K, Hirose M. Effects of N-acetylcysteine, quercetin, and phytic acid on spontaneous hepatic and renal lesions in LEC rats. *Toxicol Pathol* 2005;33:584–592.
  21. Levy E, Brunet S, Alvarez F, Seidman E, Bouchard G, Escobar E, Martin S. Abnormal hepatobiliary and circulating lipid metabolism in the Long-Evans Cinnamon rat model of Wilson's disease. *Life Sci* 2007;80:1472–1483.
  22. Huster D, Purnat TD, Burkhead JL, Ralle M, Fiehn O, Stuckert F, Olson NE, Teupser D, Lutsenko S. High copper selectively alters lipid metabolism and cell cycle machinery in the mouse model of Wilson disease. *J Biol Chem* 2007;282:8343–8355.
  23. Pierson H, Muchenditsi A, Kim BE, Ralle M, Zachos N, Huster D, Lutsenko S. The function of ATPase copper transporter ATP7B in intestine. *Gastroenterology* 2018;154:168–180.e5.
  24. Tetri LH, Basaranoglu M, Brunt EM, Yerian LM, Neuschwander-Tetri BA. Severe NAFLD with hepatic necroinflammatory changes in mice fed trans fats and a high-fructose corn syrup equivalent. *Am J Physiol Gastrointest Liver Physiol* 2008;295:G987–G995.
  25. Kleiner DE, Brunt EM, Van Natta M, Behling C, Contos MJ, Cummings OW, Ferrell LD, Liu YC, Torbenson MS, Unalp-Arida A, Yeh M, McCullough AJ, Sanyal AJ, Nonalcoholic Steatohepatitis Clinical Research Network. Design and validation of a histological scoring system for nonalcoholic fatty liver disease. *Hepatology* 2005;41:1313–1321.
  26. Tao TY, Gitlin JD. Hepatic copper metabolism: insights from genetic disease. *Hepatology* 2003;37:1241–1247.
  27. Nobili V, Siotto M, Bedogni G, Rava L, Pietrobattista A, Panera N, Alisi A, Squitti R. Levels of serum ceruloplasmin associate with pediatric nonalcoholic fatty liver disease. *J Pediatr Gastroenterol Nutr* 2013;56:370–375.
  28. Aigner E, Strasser M, Haufe H, Sonnweber T, Hohla F, Stadlmayr A, Solioz M, Tilg H, Patsch W, Weiss G, Stickel F, Datz C. A role for low hepatic copper concentrations in nonalcoholic fatty liver disease. *Am J Gastroenterol* 2010;105:1978–1985.
  29. Sternlieb I. Electron microscopy of mitochondria and peroxisomes of human hepatocytes. *Prog Liver Dis* 1979;6:81–104.
  30. Roberts EA, Robinson BH, Yang S. Mitochondrial structure and function in the untreated Jackson toxic

- milk (tx-j) mouse, a model for Wilson disease. *Mol Genet Metab* 2008;93:54–65.
31. Serviddio G, Bellanti F, Tamborra R, Rollo T, Romano AD, Giudetti AM, Capitanio N, Petrella A, Vendemiale G, Altomare E. Alterations of hepatic ATP homeostasis and respiratory chain during development of non-alcoholic steatohepatitis in a rodent model. *Eur J Clin Invest* 2008;38:245–252.
  32. McGarry JD, Foster DW. Ketogenesis and cholesterol synthesis in normal and neoplastic tissues of the rat. *J Biol Chem* 1969;244:4251–4256.
  33. Koliaki C, Szendroedi J, Kaul K, Jelenik T, Nowotny P, Jankowiak F, Herder C, Carstensen M, Krausch M, Knoefel WT, Schlensak M, Roden M. Adaptation of hepatic mitochondrial function in humans with non-alcoholic fatty liver is lost in steatohepatitis. *Cell Metab* 2015;21:739–746.
  34. Bandmann O, Weiss KH, Kaler SG. Wilson's disease and other neurological copper disorders. *Lancet Neurol* 2015;14:103–113.
  35. Czlonkowska A, Gromadzka G, Chabik G. Monozygotic female twins discordant for phenotype of Wilson's disease. *Mov Disord* 2009;24:1066–1069.
  36. Medici V, Weiss KH. Genetic and environmental modifiers of Wilson disease. *Handb Clin Neurol* 2017;142:35–41.
  37. Schiefermeier M, Kollegger H, Madl C, Polli C, Oder W, Kuhn H, Berr F, Ferenci P. The impact of apolipoprotein E genotypes on age at onset of symptoms and phenotypic expression in Wilson's disease. *Brain* 2000;123:585–590.
  38. Litwin T, Gromadzka G, Czlonkowska A. Apolipoprotein E gene (APOE) genotype in Wilson's disease: impact on clinical presentation. *Parkinsonism Relat Disord* 2012;18:367–369.
  39. Rodo M, Czlonkowska A, Pulawska M, Swiderska M, Tarnacka B, Wehr H. The level of serum lipids, vitamin E and low density lipoprotein oxidation in Wilson's disease patients. *Eur J Neurol* 2000;7:491–494.
  40. Seessle J, Gohdes A, Gotthardt DN, Pfeiffenberger J, Eckert N, Stremmel W, Reuner U, Weiss KH. Alterations of lipid metabolism in Wilson disease. *Lipids Health Dis* 2011;10:83.
  41. Ralle M, Huster D, Vogt S, Schirrmeister W, Burkhead JL, Capps TR, Gray L, Lai B, Maryon E, Lutsenko S. Wilson disease at a single cell level: intracellular copper trafficking activates compartment-specific responses in hepatocytes. *J Biol Chem* 2010;285:30875–30883.
  42. Newman JC, He W, Verdin E. Mitochondrial protein acylation and intermediary metabolism: regulation by sirtuins and implications for metabolic disease. *J Biol Chem* 2012;287:42436–42443.
  43. Menzies KJ, Zhang H, Katsyuba E, Auwerx J. Protein acetylation in metabolism - metabolites and cofactors. *Nat Rev Endocrinol* 2016;12:43–60.
  44. Hirschey MD, Shimazu T, Jing E, Grueter CA, Collins AM, Auizerat B, Stancakova A, Goetzman E, Lam MM, Schwer B, Stevens RD, Muehlbauer MJ, Kakar S, Bass NM, Kuusisto J, Laakso M, Alt FW, Newgard CB, Farese RV Jr, Kahn CR, Verdin E. SIRT3 deficiency and mitochondrial protein hyperacetylation accelerate the development of the metabolic syndrome. *Mol Cell* 2011;44:177–190.
  45. Arguello G, Balboa E, Arrese M, Zanlungo S. Recent insights on the role of cholesterol in non-alcoholic fatty liver disease. *Biochim Biophys Acta* 2015;1852:1765–1778.
  46. Schulz S, Schmitt S, Wimmer R, Aichler M, Eisenhofer S, Lichtmanegger J, Eberhagen C, Artmann R, Tookos F, Walch A, Krappmann D, Brenner C, Rust C, Zischka H. Progressive stages of mitochondrial destruction caused by cell toxic bile salts. *Biochim Biophys Acta* 2013;1828:2121–2133.
  47. Hohenester S, Gates A, Wimmer R, Beuers U, Anwer MS, Rust C, Webster CRL. Phosphatidylinositol-3-kinase p110 $\gamma$  contributes to bile salt-induced apoptosis in primary rat hepatocytes and human hepatoma cells. *J Hepatol* 2010;53:918–926.
  48. Weiss J. Haus- und versuchstierpflege: 80 Tabellen: Enke, Stuttgart, Germany 2003.
  49. Schosinsky KH, Lehmann HP, Beeler MF. Measurement of ceruloplasmin from its oxidase activity in serum by use of o-dianisidine dihydrochloride. *Clin Chem* 1974;20:1556–1563.
  50. Erel O. Automated measurement of serum ferroxidase activity. *Clin Chem* 1998;44:2313–2319.
  51. Ishak K, Baptista A, Bianchi L, Callea F, De Groote J, Gudat F, Denk H, Desmet V, Korb G, MacSween RN, et al. Histological grading and staging of chronic hepatitis. *J Hepatol* 1995;22:696–699.
  52. Zischka H, Larochette N, Hoffmann F, Hamoller D, Jagemann N, Lichtmanegger J, Jennen L, Muller-Hocker J, Roggel F, Gottlicher M, Vollmar AM, Kroemer G. Electrophoretic analysis of the mitochondrial outer membrane rupture induced by permeability transition. *Anal Chem* 2008;80:5051–5058.
  53. Schmitt S, Saathoff F, Meissner L, Schropp EM, Lichtmanegger J, Schulz S, Eberhagen C, Borchard S, Aichler M, Adamski J, Plesnila N, Rothenfusser S, Kroemer G, Zischka H. A semi-automated method for isolating functionally intact mitochondria from cultured cells and tissue biopsies. *Anal Biochem* 2013;443:66–74.
  54. Schulz S, Lichtmanegger J, Schmitt S, Leitzinger C, Eberhagen C, Einer C, Kerth J, Aichler M, Zischka H. A protocol for the parallel isolation of intact mitochondria from rat liver, kidney, heart, and brain. *Methods Mol Biol* 2015;1295:75–86.
  55. Muller FL, Liu Y, Abdul-Ghani MA, Lustgarten MS, Bhattacharya A, Jang YC, Van Remmen H. High rates of superoxide production in skeletal-muscle mitochondria respiring on both complex I- and complex II-linked substrates. *Biochem J* 2008;409:491–499.
  56. Schmitt S, Schulz S, Schropp EM, Eberhagen C, Simmons A, Beisker W, Aichler M, Zischka H. Why to compare absolute numbers of mitochondria. *Mitochondrion* 2014;19:113–123.
  57. Saggerson ED, Carpenter CA. Carnitine palmitoyl-transferase in liver and five extrahepatic tissues in the rat.



- Inhibition by DL-2-bromopalmitoyl-CoA and effect of hypothyroidism. *Biochem J* 1986;236:137–141.
58. Williams AJ, Coakley J, Christodoulou J. Automated analysis of mitochondrial enzymes in cultured skin fibroblasts. *Anal Biochem* 1998;259:176–180.
  59. Hackenbrock CR. Ultrastructural bases for metabolically linked mechanical activity in mitochondria. II. Electron transport-linked ultrastructural transformations in mitochondria. *J Cell Biol* 1968;37:345–369.
  60. von Toerne C, Kahle M, Schafer A, Ispiryanyan R, Blindert M, Hrabe De Angelis M, Neschen S, Ueffing M, Hauck SM. Apoe, Mbl2, and Psp plasma protein levels correlate with diabetic phenotype in NZO mice—an optimized rapid workflow for SRM-based quantification. *J Proteome Res* 2013;12:1331–1343.
  61. Obermann J, Priglinger CS, Merl-Pham J, Geerlof A, Priglinger S, Gotz M, Hauck SM. Proteome-wide identification of glycosylation-dependent interactors of galectin-1 and galectin-3 on mesenchymal retinal pigment epithelial (RPE) cells. *Mol Cell Proteomics* 2017;16:1528–1546.
  62. Hachmoller O, Aichler M, Schwamborn K, Lutz L, Werner M, Sperling M, Walch A, Karst U. Element bioimaging of liver needle biopsy specimens from patients with Wilson's disease by laser ablation-inductively coupled plasma-mass spectrometry. *J Trace Elem Med Biol* 2016;35:97–102.
  63. Bandow NL, Gallagher WH, Behling L, Choi DW, Semrau JD, Hartsel SC, Gilles VS, Dispirito AA. Isolation of methanobactin from the spent media of methane-oxidizing bacteria. *Methods Enzymol* 2011;495:259–269.
  64. Bradford MM. A rapid and sensitive method for the quantitation of microgram quantities of protein utilizing the principle of protein-dye binding. *Anal Biochem* 1976;72:248–254.
- 
- Received April 12, 2018. Accepted December 13, 2018.**
- Correspondence**  
Address correspondence to: Hans Zischka, PhD, Institute of Molecular Toxicology and Pharmacology, Helmholtz Center Munich, German Research Center for Environmental Health, 85764 Neuherberg, Germany. e-mail: zischka@helmholtz-muenchen.de; fax: (49) 89-4140-3412.
- Acknowledgments**  
The authors would like to thank Dr E.E. Rojo for critical reading of the manuscript.
- Author contributions**  
Claudia Einer and Christin Leitzinger performed experiments, analyzed data, and wrote the paper; Josef Lichtmanegger, Tamara Rieder, Sabine Borchard, Ralf Wimmer, and Andreas E. Kremer performed experiments; Frauke Neff, Bastian Popper, Carola Eberhagen, Elena V. Polishchuk, and Roman S. Polishchuk performed histochemical and transmission electron microscope analyses; Christine von Toerne and Stefanie M. Hauck performed the proteome analysis; Uwe Karst and Jennifer-Christin Müller performed laser ablation inductively coupled plasma-mass spectrometry; Alan A. DiSpirito, Bipin S. Baral, and Jeremy Semrau produced the methanobactin samples; Gerald Denk reviewed the data and the manuscript; Karl Heinz Weiss analyzed the data and designed experiments; Simon Hohenester analyzed the data, designed experiments, guided data compilation, and wrote the paper; and Hans Zischka designed experiments, analyzed the data, wrote the paper, and directed this study.
- Conflicts of interest**  
The authors disclose no conflicts.
- Funding**  
This study was supported in part by Deutsche Forschungsgemeinschaft grants ZI1386/2-1 (H.Z.) and HO4460/3-1 (S.H.), and by Verein zur Förderung von Wissenschaft und Forschung at the Faculty of Medicine, LMU Munich, grant 7/16 (S.H.).